Article:
Liu, J, Cao, J, He, T et al. (2022) Lacustrine redox variations in the Toarcian Sichuan Basin across the Jenkyns Event. Global and Planetary Change, 215. 103860. p. 103860. ISSN: 0921-8181

https://doi.org/10.1016/j.gloplacha.2022.103860

Lacustrine redox variations in the Toarcian Sichuan Basin across the Jenkyns Event

Jinchao Liu[a], Jian Cao[a,] *, Tianchen He[b], Feng Liang[c], Jing Pu[d], Yan Wang[a]

a. School of Earth Sciences and Engineering, Nanjing University, Nanjing 210023, China.

b. School of Earth and Environment, University of Leeds, Leeds LS2 9JT, UK.

c. Branch of Gas Production Management in Northern Central Basin, Southwest Oil and Gas Field Company, Suining 629000, China

d. Branch of Central Basin Exploration and Exploitation, Southwest Oil and Gas Field Company, Suining 629000, China

** Corresponding author. E-mail address: jcao@nju.edu.cn (J. Cao).*

ABSTRACT

The Early Jurassic Jenkyns Event (~183 Ma) represents a major environment perturbation event, characterized by the negative carbon isotope excursion during the early Toarcian. Reconstruction of redox conditions, especially in the mega-lakes, across the Jenkyns Event is of significance to understand the biogeochemical dynamics on land at the time. Here, we report iron speciation and trace metal data from the two drill cores (LQ104X and X3 wells) with different depositional environments in the lacustrine Sichuan Basin of SW China. Results show that the water column in the Sichuan Basin experienced a significant shift of redox conditions in the Toarcian. Frequent development of anoxic-ferruginous conditions,

interspersed with significant euxinic episodes across the Jenkyns Event. Conversely, during the pre/post-Jenkyns Event interval, dominantly oxic conditions, with short-lived anoxic-ferruginous or euxinic conditions, developed in the water column of the Sichuan Basin. We then proposed three possible mechanisms interdependent in nature that could have induced the water-column redox variability in Toarcian lakes: (1) lake stratifications, (2) enhanced methane release from the lake floor under low sulfate conditions that exhausted bottom water oxygen, and (3) lake eutrophication. We further anticipated that a close link between redox shift and ecological stress in the Sichuan Basin across the Jenkyns Event.

Keywords: Lower Jurassic Da'anzhai Member; lacustrine redox change; Fe speciation; P cycling; trace metal

1. Introduction

The Jenkyns Event refers to a major environmental shift that marine anoxia expanded and intensified at around 183 Ma during the early Toarcian of Early Jurassic (Jenkyns, 2010; Müller et al., 2017; Robinson et al., 2017; Reolid et al., 2020, 2021), and coincided with many other major environmental perturbations (e.g., the activity of the Karoo-Ferrar LIPs, greenhouse climate, and mass extinctions). Thus, the study of the early Toarcian oceanic anoxic event has been highlighted in the Earth system community for decades. Recently, this concept expanded to the terrestrial system (Jenkyns, 2010; Xu et al., 2017b, 2018, 2021; Liu et al., 2020; Jin et al., 2020), as the contemporaneous global carbon cycle was also perturbed and manifested in both marine and terrestrial records with a large negative carbon isotope excursion event through the Jenkyns Event (Hesselbo, et al., 2000; Kemp et al., 2005; McElwain et al., 2005; Svensen et al., 2007; Jenkyns, 2010; Percival et al., 2015, 2016; Xu et al., 2018, 2021). However, previous studies mainly focused on marine environmental responses (Pálfy and Smith, 2000; Suan et al., 2010; Jenkyns, 2010; Gómez et al., 2016; Rothman, 2017; Clarkson et al., 2018; Xu et al., 2018; Fernandez et al., 2021), and little is known regarding the responses on the lake system. Hence the investigation of the Jenkyns Event in the terrestrial realm is of great significance to understand how a hyperthermal event interacted with the terrestrial environment and ecosystem (Jenkyns et al., 2002; Burgess et al., 2015; Korte et al., 2015; Bond and Grasby, 2017; Ivanov et al., 2017; Bond and Sun, 2020; Fernandez et al., 2021; Scotese et al., 2021).

Previous analyses of marine redox conditions have suggested that widespread expansion of anoxia synchronous with the Jenkyns Event and turnovers of many benthic macrofauna and microfauna (Mattoli et al., 2008; Rita et al., 2016; Rothman, 2017; Them et al., 2018; Xu et

al., 2018; Reolid et al., 2019). The determination of lacustrine redox conditions is equally crucial because physical thermal stratification and eutrophication under hyperthermal conditions would also have impacted the redox gradient in large lake systems (Scholz, 2018) and led to a significant shift in the "habitability for lake ecosystem". In addition, redox conditions in lakes also influence the biogeochemical cycling of key nutrient elements such as phosphorus (Kraal et al., 2012). Thus, the benthic cycling of P and productivity link to water-column redox conditions (Kraal et al., 2012; Xiong et al., 2019; Schobben et al., 2020).

The Sichuan Basin is a large, lake basin in southwest China, in which the Lower Jurassic Da'anzhai Member recorded the Jenkyns Event (Li et al., 2013). The Sichuan Basin offers a good window to investigate lacustrine redox changes in the water column across the Jenkyns Event (Xu et al., 2017a, 2021; Liu et al., 2020). Xu et al. (2017a) applied redox-sensitive element pairs (i.e., Ni/Co, Th/U, V/Cr, and V/Sc) and δCe ($\delta Ce = Ce_N / (La_N \times Pr_N)^{1/2}$) to preliminarily reconstruct the redox condition of the entire Da'anzhai Member in the Sichuan Basin, which indicates the dominantly oxic-suboxic condition. Based on the enrichment factor of Mo (Mo_{EF}) and the occurrence of pyrite in the Da'anzhai Member, Xu et al. (2017b) suggested that the Sichuan Basin may have developed some euxinic condition during the early Toarcian, but the exact timing, extent and geographic spread of these extreme anoxic conditions remain unclear. Liu et al. (2020) demonstrated that the Sichuan Basin was poised at oxygen-deficiency during the Jenkyns Event by utilizing Mo_{EF} and the molar ratios of organic carbon to total phosphorus (C_{org}/P_T). These interpretations are not unified, and are limited to single sedimentary environments, therefore, pending on more robust and direct water column redox proxy (e.g., Fe speciation) to trace lacustrine redox changes across specific timelines over areas sufficiently large to constrain basin-scale dynamics (Gilleaudeau et al., 2021).

These uncertainties also limit the understanding of mechanisms that drove the occurrence, expansion, and contraction of oxygen-deficiency in the basin, and further restrict the disclosure of the mechanism of the Jenkyns Event on land.

Here, we present new water column redox proxy data (Fe speciation and trace metals) from the organic-rich mudstone deposition of the Da'anzhai Member of 2 drill cores, which covers a basin transect from deep lacustrine to shallow lacustrine settings during the early Toarcian. Our study provides an important example of water column redox changes in paleo-lake basins across an extreme hyperthermal event (Jenkyns Event). The results shed new light on the lateral water-mass geochemistry variability across the Sichuan Basin and the dynamic lacustrine redox conditions.

2. Geological setting

The modern Sichuan Basin is located in southern China with a total area of ca. 230, 000 km^2, and its margins were surrounded by three mountain ranges, except for the southern part, during the Early Jurassic (Zhu et al., 2007; Zhao et al., 2010; Liu, et al., 2020; Fig. 1a). The paleo-Sichuan Basin in the Early Jurassic has been suggested to be larger than its present confines, and its maximum depth was greater than 200 m (Xu et al., 2020).

The Sichuan Basin entered a terrestrial setting since the Late Triassic (Li and He, 2014). During the Early Jurassic, lacustrine deposits, mainly the Ziliujing Formation, formed in the centre of the basin located in the Yingshan–Yilong area (Zhao et al., 2010; Li et al., 2013; Feng et al., 2015), which can be divided into the Zhenzhuchong, Dongyuemiao, Ma'anshan, and Da'anzhai members from bottom to top. Based on micro- and macrofossil biostratigraphy, carbonisotope chemostratigraphy and Re-Os geochronology, Xu et al. (2017b) established a

stratigraphic framework for the Da'anzhai Member in the Sichuan Basin, suggesting that deposition of this lacustrine succession have directly coincided with the Jenkyns Event (ca. 180 ± 3.2 Ma), corresponding to the late *tenuicostatum–falciferum* (*serpentinum*) zone of the ammonite province in northern European (Jenkyns, 1985).

The Da'anzhai Member can be mainly divided into the shelly beach, shallow lake, semi-deep lake and deep lake subfacies based on the previously reported petrographic and sedimentary evidence (Li et al., 2013; Li and He, 2014). The Da'anzhai Member occurs continuously throughout the Sichuan Basin, which was deposited during a complete lacustrine shallowing–deepening cycle, and formed a series of shell-bearing limestone–mudstone rocks (Zheng et al., 1998; Wang et al., 2004; Li et al., 2013; Feng et al., 2015; Liu et al., 2020). From base to top, it can be divided into lower siltstone and/or silty mudstone, lower coquina, (shell-bearing) mudstone, upper coquina, and upper silty mudstone and/or siltstone (Liu et al., 2020). The silty mudstone and siltstone formed in the offshore–shallow lacustrine facies, the coquina formed in the shelly beach facies, and the (shell-bearing) mudstone formed in the semi-deep or deep lacustrine facies (Li and He, 2014; Feng et al., 2015).

3. Samples and methods

The studied core samples (n= 107) are collected from two representative wells: LQ104X (N 31°18′57″, E 106°49′06″) and X3 (N 30°43′43″, E 105°53′26″) (Fig. 1b, c). The LQ104X well is located approximately 42 km southwest of Pingchang County, while the X3 well is located approximately 20 km southeast of Pengxi County (Fig. 1b). The samples from LQ104X well were deposited in deep or semi-deep lacustrine facies, while samples from X3 well were mainly deposited in shallower lacustrine facies. Rock samples were crushed and

powered using a silica mill in order to obtain a homogeneous powder. It is noteworthy that the data of organic carbon isotopes, and major and trace elements of LQ104X well are presented from a previous work (Liu et al., 2020). New data include total organic carbon (TOC) contents and Fe speciation of LQ104X and X3 wells, organic carbon isotopes and major and trace elements of X3 well.

3.1. TOC and organic carbon isotope $\delta^{13}C_{org}$ analysis

Total organic carbon contents were conducted with an Elementar Vario Macro CHNS element analyzer at the MOE Key Laboratory of Surficial Geochemistry at Nanjing University. The powder samples were treated with 2 M HCl at 60 °C for 24 h to remove inorganic carbon, and then rinsed with distilled water five times and dried for 72 h to remove the excess HCl. Analytical uncertainties were estimated to be < 5%.

Organic carbon isotopes were determined with a Finnigan MAT 253 mass spectrometer at the State Key Laboratory for Mineral Deposits Research at Nanjing University. The powdered organic carbon samples were evenly mixed with CuO powder (mass ratio of 1:8) in a quartz tube, vacuum sealed, and heated at 850 °C. After cooling in a cryotrap to separate H_2O, CO_2 was introduced directly into the inlet system of the mass spectrometer. The results are reported in standard per mil (δ) notation relative to Vienna Peedee Belemnite (VPDB). The black carbon standard GBW04407 ($\delta^{13}C_{VPDB} = -22.43‰ \pm 0.07‰$) was used as the reference standard, and the precision of the measurements was ± 0.1‰.

3.2. Major and trace element analysis

Dried powdered samples (ca. 50 mg) were subjected to total digestion using an HF-HNO_3

mixture in high-pressure Teflon bombs under 190 °C temperature. The resulting solution was then measured for major elements concentrations using Thermo iCAP 6300 inductively coupled plasma optical emission spectrometer (ICP-OES) at the MOE Key Laboratory of Surficial Geochemistry at Nanjing University, and trace elements concentrations using Aurora M90 inductively coupled plasma mass spectrometer (ICP-MS) at the State Key Laboratory for Mineral Deposits Research at Nanjing University. Rh was used as an internal standard to monitor the signal drift during measurements. Elemental concentrations were calibrated with the USGS rock standards GSP-1 and AGV-2. Analytical uncertainties were estimated to be < 10%.

3.3. Fe speciation analysis

A sequential extraction scheme was applied to determine operationally defined pools of reactive Fe minerals (Fe_{HR}) in sediment samples, including carbonate associated iron (Fe_{Carb}), pyrite (Fe_{Py}), ferric oxides (Fe_{Ox}) and magnetite (Fe_{Mag}) (Poulton and Canfield, 2005). The powder sample (ca. 100 mg) was first treated with CH_3COONa solution at pH 4.5 and 50 °C for 48 h to extract Fe_{Carb}. Fe_{Ox} was then extracted via $Na_2S_2O_4$ solution at pH 4.8 and at room temperature for 2 h. This is followed by the final leaching of Fe_{Mag} with $(NH_4)_2C_2O_4$ solution at room temperature for 6 h. Extraction solutions were analyzed for Fe concentration by thermos iCAP 6300 ICP-OES with Y as an internal standard at the MOE Key Laboratory of Surficial Geochemistry at Nanjing University. The Fe concentrations were calibrated with the GSB 04-1726-2004. Analytical uncertainties were estimated to be < 10%. Concentrations of Fe_{Py} were determined by the Cr reduction method (Alcott et al., 2020), and were calculated stoichiometrically by the weight of precipitated Ag_2S from the extraction.

3.4. Calculation of trace metal enrichment factors

To constrain the sedimentary enrichment degree of the trace elements relative to continental crust, the "enrichment factors" (EFs) were calculated (SupplementaryTable 1) (Tribovillard et al., 2006; Algeo and Tribovillard, 2009; Algeo and Liu, 2020). The EFs are defined as: $X_{EF} = \frac{(\frac{X}{Al})_{sample}}{(\frac{X}{Al})_{UCC}}$, where X and Al represent the weight% concentrations of elements X and Al, respectively (Tribovillard et al., 2013) and UCC is Upper Continental Crust (Rudnick and Gao, 2014). X_{EF} less than 1 and greater than 1 imply that element X is depleted and enriched relative to UCC, respectively (Tribovillard et al., 2006).

3.5. Calculations of Chemical index of alternation

The intensity of regional terrestrial weathering can be determined by the chemical index of alteration (CIA) in sedimentary rocks, which was first proposed by Nesbitt and Young (1982) and defined as:

$$CIA = \frac{Al_2O_3}{Al_2O_3 + CaO^* + Na_2O + K_2O} \times 100,$$

where CaO* represents the CaO in silicate mineral, defined as $CaO^* = CaO - (\frac{10}{3} \times P_2O_5)$. If the $CaO^* < Na_2O$ (mole fraction), the CaO* is used, otherwise, the Na_2O is used as CaO* in the calculation of CIA. Note that, the CIA parameter applies to mudstone/shale, thus the (clay-bearing) coquina samples with greater than 30 wt. % $CaCO_3$ content are not included in the following discussion.

4. Results

4.1. TOC, and $\delta^{13}C_{org}$

197 The TOC contents of the samples range from 0.06–2.69 wt.%, with an average of 0.95
198 wt.% (Supplement Table 1). The TOC contents in LQ104X well (0.06–2.69 wt.%, mean =
199 1.03 wt.%) is slightly higher than that of X3 well (0.06–2.45 wt.%, mean = 0.87wt.%). The
200 $\delta^{13}C_{org}$ values of the samples in X3 well range from –33.2– –22.7 ‰, with an average of –
201 27.8 ‰.
202
203 ***4.2. Major and trace elements***
204 The average of Ca (12.3 wt.%) and Al (8.07 wt.%) contents of samples in X3 well is
205 generally higher than the other elements in the Da'anzhai Member (Supplement Table 1). The
206 fluctuation of Ca (range from 0.23–44.5 wt.%) contents is more obvious than that of Al (range
207 from 0.86–11.8 wt.%). Additionally, the average of Ti, Fe, Mg, Na, K and P contents in X3
208 well is 0.33 wt.%, 3.99 wt. %, 1.54 wt.%, 0.33 wt.%, 2.03 wt.% and 0.07 wt.%, respectively
209 (Supplement Table 1).
210 The Mo, U and Zr contents of samples in X3 well range from 0.48–5.81 ppm (mean =
211 1.70 ppm), 0.60–4.5 ppm (mean = 2.66) and 11.9–212 ppm (mean = 110 ppm), respectively
212 (Supplement Table 1).
213
214 ***4.3. Fe speciation***
215 The average of Fe_{HR} contents in X3 well (mean = 1.34 wt.%) is slightly higher than that
216 in LQ104X well (mean = 1.22 wt.%). Among the Fe_{HR} speciation, the contents of Fe_{Py} (mean
217 = 0.54) in two wells are the highest. The average of Fe_{Carb}, Fe_{Ox} and Fe_{Mag} contents of all
218 samples is 0.37 wt.%, 0.14 wt.% and 0.24 wt.%, respectively (Supplement Table 1). The
219 contents of Fe_{Py} in LQ104X well (mean = 0.58 wt.%) is slightly higher than that in X3 well

(mean = 0.51 wt.%).

5. Discussion

5.1. The comparison of the carbon isotope stratigraphy

The Jenkyns Event is characterized by a prominent combination of negative carbon isotope excursions (CIEs) and organic matter accumulation (high TOC contents) in the marine sedimentary records due to massive injection of the isotope-light carbon (^{12}C-rich) to the atmosphere–marine system (Duncan et al., 1997; Hesselbo, et al., 2000; Kemp et al., 2005; McElwain et al., 2005; Svensen et al., 2007; Jenkyns, 2010; Percival et al., 2015, 2016; Suan et al., 2015; Xu et al., 2018, 2021; Ruebsam et al., 2020). Nonetheless, the CIE is synchronously preserved in the fossil woods sourced from terrestrial realms (Hesselbo et al., 2007, 2011). Moreover, the contemporary Sichuan Basin and Ordos Basin, where expanded lake systems were developed, also archive this major carbon cycle perturbation event (Xu et al., 2017b; Jin et al., 2020). In this study, our organic carbon isotope record from both wells in the Sichuan Basin show a negative $\delta^{13}C_{org}$ excursion with a magnitude of 4.1‰ (–24.6 – –28.4‰) in the shallower X3 well, and 3.8‰ (–24.6 – –28.4‰) in the deep water LQ104X well. These excursions are also accompanied by a significant increase in TOC abundances by 2.3% in the shallower X3 well and 2.6% in the deep water LQ104X well (Fig. 2). Both the absolute values and magnitude of the excursion are consistent with those observed in early Toarcian marine and terrestrial organic-matter records from Europe (i.e., Mochras Borehole in the UK) and the Sichuan Basin through the Jenkyns Event (Core A in Xu et al., 2017b, 2018; LQ104X well in Liu et al., 2020). Importantly, the X3 well, LQ104X well, and reported Core A share the same lithological units (Da'anzhai Member), i.e., alternating beds of fossiliferous

carbonate and dark mudrocks from clay-rich marl to laminated black shale. (Fig. 2; Xu et al., 2017b, 2021; Liu et al., 2020). This provides the basis for the comparison of carbon isotope stratigraphy in the present study. Note that, there is also an obvious negative CIE in the 1769.75–1781.33 m interval of X3 well. However, this negative CIE is accompanied by extremely low TOC contents (mean = 0.18 wt. %) instead of high TOC contents. The thickness of the Jenkyns Event intervals of the classical Peniche section is ca. 35 m (Hesselbo et al., 2007), sharply greater than ca. 12m of the X3 well (1769.75–1781.33 m). Given that the sedimentary rate in lake systems is higher than that in ocean systems, the thickness of the Jenkyns Event interval in lake systems should be expected to be greater than 30 m. Therefore, we argue that the 1782.2–1822.2 m interval (40 m) of the X3 well responds to the Jenkyns Event rather than the 1769.75–1781.33 m interval (ca. 12 m).

5.2. Toarcian Terrestrial input in the Sichuan Basin

Elevated terrestrial weathering rate and terrigenous input were observed in many proximal marine and lacustrine sites on a global scale during the Jenkyns Event (Cohen et al., 2004; Jenkyns, 2010; Dera et al., 2011; Kemp et al., 2011; Brazier et al., 2015; Percival et al., 2016; Them et al., 2017; Izumi et al., 2018; Xu et al., 2018). Hence, it is crucial to assess the potential weathering influence on various elemental enrichments in the Toarcian sediments of the Sichuan Basin, especially for the periphery of the Sichuan Basin where terrigenous input may have been strengthened during the Jenkyns Event (Xu et al., 2018). During the process of chemical weathering on land, calcium (Ca), sodium (Na) and potassium (K) that assemble the CIA proxy generally are removed from the feldspars such that the proportion of alumina (Al) to alkalis usually increases in the weathered end-product (Nesbitt and Young, 1982). Thus, the

CIA can assess the regional terrestrial chemical weathering intensity of hinterland around the periphery of the Sichuan Basin. Additionally, aeolian inputs is also a potential source of elements in the lake or marginal marine-setting. The grain-size distribution of the lithogenous fraction of sediments can be used to derive relative wind strengths on the assumption that more vigorous atmospheric circulation will transport larger particles (mineral and rock grains) to a given site of deposition. Some geochemical proxies such as Ti/Al and Zr/Al have been successfully used to track aeolian inputs. (Calvert and Pedersen, 2007).

CIA values through the Da'anzhai Member in two wells of this study range from 50.1–83.2, with an average of 68.1. Among them, average CIA values in the deeper LQ104X well (mean = 75.2) yield a higher level than those of X3 well (mean = 68.1). These high background CIA (> 65) values in the Sichuan Basin confirm the indication of a warm climate during the early Toarcian, associated with a moderate chemical weathering intensity (Nesbitt and Young, 1982; Fedo et al., 1996; Young and Nesbitt, 1999; Guo et al., 2018). Note that, the CIA values at 1769.75–1781.33 m interval of X3 well is ineffective due to their host-rock lithology of coquina or limestone with high Ca contents and low Al contents. Additionally, the CIA record shows an upward decreasing trend in the deep water LQ104X well (Fig. 3A), but remains relatively stable through the succession in the shallower X3 well (Fig. 3B). No sudden rise in CIA values was observed in these records associated with the Jenkyns Event. Similarly, the Ti/Al and Zr/Al ratios also show an upward decreasing trend in the Jenkyns Event interval of both the LQ104X and X3 wells. Such features may indicate that the contemporaneous weathering conditions in the early Toarcian may have not exerted a major control over raw material and nutrient delivery to the periphery of the Sichuan Basin at a regional scale. Hence, we argue that terrigenous input had a minor influence on elemental enrichment in lacustrine

sediments (e.g., highly reactive iron and trace metal) adjacent to the hinterland. Indeed, no covariation was present between CIA, Ti/Al and Zr/Al with Fe_{HR}/Fe_T and Mo/U at both the proximal X3 well and deeper water LQ104X, which possibly indicates domination of lacustrine redox control rather than terrestrial input.

5.3. Early Toarcian lacustrine redox change in the Sichuan Basin

Having established that the iron speciation and trace metal concentrations in these lacustrine sediments likely receive minimal terrestrial influence, here we utilize Fe speciation and trace metal to track the variation of lacustrine redox condition in the water column of the Sichuan Basin through the early Toarcian. The calibration of modern sediments and ancient sedimentary rocks indicates that aquatic sediments may enrich in Fe_{HR} in an anoxic water column ($Fe_{HR}/Fe_T > 0.22–0.38$) compared to oxic conditions (Poulton and Raiswell, 2002; Poulton et al. 2010; Raiswell and Canfield, 2012; Clarkson et al., 2014; Them et al., 2018; Stüeken et al., 2019; Poulton, 2021). However, it is noteworthy that these thresholds for distinguishing anoxic conditions in marine deposits may vary significantly in lacustrine environments due to more restricted settings in lakes. Additionally, the enrichment of U can provide independent constraints on the redox condition. U exists as a soluble UO_2^{2+} in the oxidized water column. Under the reducing condition, the U(VI) will be reduced to less soluble U(IV) (i.e., UO_2, U_3O_7 and U_3O_8) and hereby promote authigenic enrichment of U in the sediments relative to the average crustal abundance (Tribovillard et al., 2008; Azrieli-Tal et al., 2014; Bura-Nakić et al., 2018; Lu, et al., 2020; He et al., 2022). The anoxic condition can be further determined by detecting the proportion of pyrite in the Fe_{HR} pool, where a ferruginous (anoxic, Fe^{2+} rich and sulfide-free) water column yields Fe_{Py}/Fe_{HR} lower than 0.6-

0.8 and euxinic condition above this threshold in the marine environment (Poulton, 2021). In addition, Mo is present in the water column as the stable and largely unreactive molybdate oxyanion (MoO_4^{2-}) in oxic conditions. Under anoxic–sulfidic conditions, the MoO_4^{2-} will be converted to thiomolybdates ($MoO_xS_{(4-x)}^{2-}$, x = 0–3), which is easy to be absorbed by organic matter or Fe sulfide, resulting in the enrichment of Mo (Algeo and Tribovillard, 2009; Bura-Nakić et al., 2018). The variation of these proxies for the two wells in this study was presented in Fig. 4 (LQ104X well) and Fig. 5 (X3 well), respectively.

In the LQ104X well (Fig. 4), sediments have no co-enrichment of U and Fe_{HR} below the 3535.95 m (Ma'anshan Member and lower Da'anzhai Member) and above the 3519.96 m (top of the Da'anzhai Member) (Fig. 4c and 4g), suggesting that oxic conditions were dominant at the time, except for a few occasions (i.e., 3546.95 m, 3512.02 m, 3501.92 m and 3496.15–3497.02 m). These periods of co-enrichment in U and Fe_{HR} (Fig. 4c and 4g) likely indicate short-lived anoxic episodes. In the 3535.95–3519.96 m (middle of the Da'anzhai Member) of the section (i.e., the nadir of the CIE), relative longer-term enrichments in U (U_{EF} above the UCC) were observed (Fig. 4g), coinciding with elevated Fe_{HR}/Fe_T ratios (Fig. 4c), which suggest that the anoxic condition prevailed in the Sichuan Basin during the heyday of the Jenkyns Event. Furthermore, the covariation between their U/Al and Fe_{HR}/Fe_T ratios supports the dominantly anoxic condition (Fig. 6a).

Moreover, several samples in the Sichuan Basin show Fe_{Py}/Fe_{HR} ratios scattering around the equivocal zone (0.6–0.8) in the 3535.95–3519.96 m section (Fig. 4d), which may indicate either anoxic-ferruginous or euxinic condition (Poulton, 2021). Furthermore, all these samples with high Fe_{Py}/Fe_{HR} ratios coincide with co-enrichment in Mo_{EF} and Mo/U (Fig. 4d, 4f, 4h and 4i), which suggests a fluctuation state between anoxic-ferruginous and euxinic conditions in

335 the water column of the Sichuan Basin during the major phase of the Jenkyns Event (Fig. 4i).
336 Additionally, co-enrichment of Fe_{Py}/Fe_{HR}, Mo_{EF} and Mo/U also occurred in the 3501.92 m and
337 3496.15–3497.02 m intervals (top of the Da'anzhai Member) indicative of short-lived euxinic
338 condition (Fig. 4d, 4f, 4h and 4i).
339 The early Toarcian redox variation in the shallower X3 well is similar to that in LQ104X
340 well (Fig. 5). Sediments have no co-enrichment of U and Fe_{HR} below the 1806.90 m (bottom
341 of the Da'anzhai Member) and above the 1795.05 m (top of the Da'anzhai Member and
342 Lianggaoshan Formation; Fig. 5c and 5g) in the X3 well, suggesting that oxic conditions were
343 dominant, except for individual intervals (i.e., 1820.8 m, 1786.50–1787.35 m, 1780.15 m and
344 1769.75 m). Co-enrichment in Fe_{HR}/Fe_T and U occurred in the 1806.90–1795.05 m section
345 (middle Da'anzhai Member), indicating a dominantly anoxic condition (Fig. 5c and 5g). There
346 is also co-enrichment in Fe_{Py}/Fe_{HR}, Mo_{EF} and Mo/U in the 1806.90–1795.05 m section of the
347 middle Da'anzhai Member (nadir of the CIE; Fig. 5d, 5f and 5h), suggesting redox fluctuation
348 between anoxic-ferruginous and euxinic conditions, consistent with the cotemporaneous redox
349 state in the deeper site (LQ104X well) (Fig. 5i).
350 In summary, the water column in the Sichuan Basin experienced a significant shift
351 towards oxygen level deterioration during the early Toarcian Jenkyns Event. Dominantly oxic
352 condition, with short-time anoxic-ferruginous interval, developed in the water column
353 preceding the Jenkyns Event (Fig. 4i and 5i). This was immediately followed by a shift
354 towards an anoxic state during the heyday of the Jenkyns Event, but it alternates between
355 anoxic-ferruginous and euxinic conditions possibly as a result of fluctuation in sulfate
356 availability (Fig.4i and 5i). Then, the water column switched back to a more oxic condition,
357 interspersed with occasionally anoxic-ferruginous or euxinic conditions in the Sichuan Basin

following the Jenkyns Event (Fig. 4i and 5i).

5.4. Development mechanism of the redox transition during the Jenkyns Event in the Sichuan Basin

Based on the above discussion, it is clear that strengthened lacustrine anoxia was developed in the Sichuan Basin during the Jenkyns Event. There may have been several possible mechanisms independently or collectively driving this major redox shift in theory, including (1) lake stratification, (2) enhanced methane release from the lake floor that exhausted bottom water oxygen, and (3) lake eutrophication (Reed et al., 2016; He et al., 2020; Woolway et al., 2021).

Global warming would have a considerable influence on lake stratification. Heat input tends to warm the near-surface layer (Woolway et al., 2021). This shifts the density in warm surface water to lower than that in deep water, hence the water column circulation is suppressed (Woolway et al., 2021). Additionally, large lake systems are more subjected to being stratified due to the enormous morphology (depth and surface area) (Xu et al., 2017b; Woolway et al., 2021). It is widely known that the average global temperature rose by 5–7°C during the Jenkyns Event (Jenkyns et al., 2002; Korte et al., 2015; Krencker et al., 2015; Bond and Grasby, 2017; Jones et al., 2018; Bond and Sun, 2020; Ruebsam et al., 2020; Fernandez et al., 2021; Scotese et al., 2021), while the Sichuan Basin had expanded to a large lake system associated with rising lake level (Xu et al., 2017b, 2021; Liu et al., 2020). Hence, the development of the anoxic condition within the Jenkyns Event may be driven by thermal stratification that was ultimately promoted by the greenhouse climate and the elevated lake-level at the time. Importantly, enhanced lake stratification in the Sichuan Basin was supported

by evidence of elevated gammacerane index during the Jenkyns Event (Xu et al., 2021).

Releasing of methane from the sediments on the lake floor to the water column may be an additional possible mechanism, as the lake system is one of the important sources of methane to the atmosphere, and the methanogenesis ($CH_3COO^- + H^+ \rightarrow CH_4 + CO_2$ and $CO_2 + 4H_2 \rightarrow CH_4 + 2H_2O$) is common in lake sediments when there is sufficient organic supply (Beaulieu et al., 2019; He et al., 2020). The anaerobic oxidation of methane (AOM: $CH_4 + SO_4^{2-} \rightarrow HCO_3^- + HS^- + H_2O$) and sulfate reduction ($SO_4^{2-} + 2CH_2O \rightarrow H_2S + 2HCO_3^-$) are dominant microbial processes in methane-rich sediments (Hinrichs and Boetius, 2002; Joye et al., 2004). One of the key features of the Jenkyns Event is the massive accumulation of organic matter (McArthur et al., 2008; Jenkyns et al., 2010; Montero-Serrano et al., 2015; Suan et al., 2015; Reolid et al., 2020). High organic carbon loading to the lake floor may enhance methane production and benthic release to the water column in the Sichuan Basin during the Jenkyns Event. The Sichuan Basin is generally a freshwater lake system with low sulfate concentrations through most of the early Toarcian, which limits the capacity for AOM (He et al., 2020; Liu et al., 2020). Suppressed AOM in the Sichuan Basin would enable elevated methane flux to escape to the water column and consume free O_2, thus inducing negative feedback on oxygen levels (Günthel et al., 2019; He et al., 2020). Consequently, the redox state in the Sichuan Basin turns to the anoxic-ferruginous condition under low sulfate settings, or euxinic conditions when sulfate supply and microbial sulfate reduction intensity were high.

Moreover, eutrophication at the epilimnion would also have resulted in the decline of oxygen level, and even euxinic, in the water column (Reed et al., 2016). Eutrophication is often regarded as the ecosystem response to increased nutrient loading. Generally,

eutrophication elevated primary productivity in surface waters due to high nutrient load, which enhances the organic matter export to the lake floor and increases benthic oxygen demand (Gustafsson et al., 2012; Carstensen et al., 2014; Reed et al., 2016). Importantly, global warming will likely accelerate existing eutrophication effects (Seidel et al., 2021), which provides a premise for the possible eutrophication in the Sichuan Basin during the Jenkyns Event. It is acknowledged that nutrient, which is usually linked to terrigenous input, is essential to eutrophication formation. Xu et al. (2017) attributed the increased productivity during the Jenkyns Event to elevated continental weathering and accelerated riverine nutrient supply. However, our data show that the intensity of regional terrestrial chemical weathering in the periphery of the Sichuan Basin was not elevated during the Jenkyns Event, based on the CIA, Ti/Al and Zr/Al data (Fig. 3). Therefore, even if eutrophication contributes to the redox shift during the Jenkyns Event in the Sichuan Basin, the increased nutrient surge may not relate to continental weathering, but via another mechanism(s) (e.g., the release of benthic phosphorus). Global warming or enhanced weathering input stimulates the formation of eutrophication and further promotes the anoxic condition in the Sichuan Basin. Additionally, increasing organic matter deposition may enhance the methanogenesis, resulting in the release of CH_4 to the water column, and further increased oxygen demand. Owing to the cooperation of the above three potential mechanisms, the redox condition in the Sichuan basin would have shifted to intesified anoxic-ferruginous or euxinic conditions, and the Jenkyns Event eventually happened.

5.5. Coupling of redox changes and benthic phosphorus cycling across the Jenkyns Event

Phosphorus (P) is a key limiting nutrient for many aquatic ecosystems (Bush et al., 2017).

Indeed, elevated inputs of P have been regarded as an important cause of high productivity (i.e., eutrophication). As mentioned above, the intensity of terrestrial weathering did not increase during the Jenkyns Event. Alternatively, we propose that increased benthic P recycling would have driven the nutrient surge. Benthic phosphorus cycling is closely related to redox conditions (Kraal et al., 2012; Kormar and Zeebe, 2017; Xiong et al., 2019; Guilbaud et al., 2020; Schobben et al., 2020). Variation in redox conditions during the Jenkyns Event had the potential to perturb the benthic P cycling and the paleo-productivity in the Sichuan Basin (Komar and Zeebe, 2017; Reinhard and Planavsky, 2020; Schobben et al., 2020).

Low C_{org}/P_T ratios occurred in pre-Jenkyns Event intervals (i.e., below the 3541.88 m in LQ104X well (average = 35.8) and 1816.25 m in X3 well (average = 24.0)) and post-Jenkyns Event intervals (i.e., above the 3519.96 m in LQ104X well and 1792.1 m in X3 well, Fig. 7). During these intervals, the water column redox condition was dominantly oxic based on trace metal and iron speciation data (Fig. 7), while P was possibly being drawdown to sediment with Fe- (oxyhydr)oxides and/or organic matter, hence P is retained in sediments with suppressed P recycling (Anderson and Sarmiento, 1994; Algeo and Ingall, 2007; Algeo and Herrmann, 2018; Xiong et al., 2019; Guilbaud et al., 2020; Schobben et al., 2020).

Higher C_{org}/P_T ratios occurred during the Jenkyns Event (i.e., 3519.96 m–3541.88 m in LQ104X well (average = 63.3) and 1792.1–1816.25 m in X3 well (average = 71.3), Fig. 7). During the Jenkyns Event, the water column was dominated by strengthened anoxia and frequent development of euxinic conditions. Beneath an anoxic-sulfidic water column, P is recycled back to the water column via effective anaerobic organic matter remineralisation. Consequently, extensive recycling of P release reactive P back to the water column, which leads to elevated C_{org}/P_T in sediments and potentially higher productivity in the surface water

(Reinhard and Planavsky, 2020; Schobben et al., 2020).

In summary, the fluctuation of P cycling during the Jenkyns Event in the Sichuan Basin may suggest that the transition of the redox state in the Sichuan Basin, and the release of benthic phosphorus is a potential cause for eutrophication in the Toarcian Sichuan Basin. Figure 8 presents the conceptual model of these changes. Oxic condition was dominant in the basin during the pre-Jenkyns Event interval. U, Mo and Fe exist as soluble UO_2^{2+} (VI), MoO_4^{2-} (VI) and Fe- (oxyhydr)oxides (III), respectively. Phosphorous may be present in association with Fe (oxyhydr) oxides. Subsequently, during the heyday of the Jenkyns Event, when the LQ104X site and X3 site are situated below the chemocline with dominantly anoxic–ferruginous or euxinic conditions. The U (VI) was reduced to U (IV), existing as less soluble UO_2. The MoO_4^{2-} was converted to thiomolybdates ($MoO_xS_{(4-x)}^{2-}$, x = 0–3), and adsorbed by organic matter or Fe sulfide. Fe (oxyhydr) oxides dissolved, and the P was released, which would induce an increase in productivity. The soluble Fe^{2+} would combine with free H_2S to form pyrite, which may facilitate the Mo enrichment. The post-Jenkyns Event interval was dominated by the oxic condition at both sites, but interspersed with short-lived anoxic pulses. The U, Mo, Fe and P would revert to their original form as before the Jenkyns Event occurred.

5.6. Implications for the relation of redox transition and ecological stress in the Sichuan Basin during the Jenkyns Event

The temperature has a fundamental effect on almost all biological activities (Brown et al., 2004). As mentioned in section 4.4, global warming would result in thermal stratification, which adds a significant impact on biological productivity by directly influencing the size of

the trophogenic zone where photosynthesis takes place and also influencing nutrient supply from deep water (O'Beirne et al., 2017; Yankova et al., 2017; Woolway et al., 2021). Additionally, transition in redox conditions will also affect biotic communities, because redox reactions can supply energy for metabolisms in the ecosystem (Zakem et al., 2020). Bush et al. (2017) present a mathematical model describing interactions between microbial and biogeochemical oxidation–reduction reactions, suggesting that this model abruptly transitions between an oxic state dominated by cyanobacteria and an anoxic state with sulfate-reducing bacteria and phototrophic sulfur bacteria. Note that, this model has been validated in the lake system (i.e., Lake Vechten; Bush et al., 2017).

In the Sichuan Basin, the kerogen type, amorphous organic matter (AOM) abundance, and TPP (C_{30} tetracyclic polyprenoids) ratios across the Jenkyns Event suggests stratigraphic changes in the composition of sedimentary organic matter towards a more hydrogen-rich, algae-derived component during the Jenkyns Event (Holba et al., 2000; Xu et al., 2021). Additionally, the high abundance of hopanes relative to steranes in the Jenkyns Event interval indicates the relatively high bacterial activity. Importantly, the presence of 3β-methylhopane, mainly derived from methane-oxidizing bacteria (Farrimond et al., 2004; Welander and Summons 2012), indicating oxidation of methane during deposition of the Da'anzhai Member (Xu et al., 2021), proved that massive methane had likely been released to the water column during the Jenkyns Event. Therefore, the redox transition and ecological community dynamics may indeed have a close link in the Sichuan Basin during the Jenkyns Event.

6. Conclusions

The trace metal and Fe speciation indicate that the water column in the Sichuan Basin

experienced the significant transition of redox condition in Toarcian (i.e., commonly oxic condition before the heyday of the Jenkyns Event, a frequent fluctuation between commonly anoxic-ferruginous and euxinic conditions in the heyday of the Jenkyns Event, and commonly oxic with the occasionally anoxic-ferruginous or euxinic condition after the heyday of the Jenkyns Event).

The possible mechanisms resulting in the transition of redox conditions in the Sichuan Basin across the Jenkyns Event include: (1) lake stratification, (2) methane release to bottom water, and (3) eutrophication, and these three controls may be essentially interdependent. The potential eutrophication induced by high nutrient load may not source from elevated terrestrial weathering but from benthic phosphorus releasing due to the redox transition during the Jenkyns Event.

There are obvious changes in the ecological system in the Sichuan Basin during the Jenkyns Event, which suggest that the relationship between redox transition and ecological community dynamics may indeed exist in the Sichuan Basin. This idea would benefit from more specific works to be further and better developed.

Declaration of competing interest

The authors declare that they have no known competing financial interests or personal relationships that could have appeared to influence the work reported in this paper.

Acknowledgements

This work was supported by the National Natural Science Foundation of China (Grant No. 41888101 to TH). This work is also a contribution to the Integrated Understanding of the

519 Early Jurassic Earth System and Timescale (JET) project and IGCP 739. Professor Guang Hu
520 and Drs Zhiwei Liao and Ruofei Yang are acknowledged for assistance in the field work.
521

522 **Appendix A. Supplementary data**

523 Supplementary data to this article can be found at Supplementary Data 1.
524
525
526

527 **References**

528 Alcott, L.J., Krause, A.J., Hammarlund, E.U., Bjerrum, C.J., Scholz, F., Xiong, Y., Hobson,
529 A.J., Neve, L., Mills, B.J.W., März, C., Schnetger, B., Bekker, A., Poulton, S.W., 2020.
530 Development of Iron Speciation Reference Materials for Palaeoredox Analysis.
531 Geostand. Geoanalytical Res. 44, 581–591. doi:10.1111/ggr.12342.
532 Algeo, T.J., Herrmann, A.D., 2018. An ancient estuarine-circulation nutrient trap: The Late
533 Pennsylvanian Midcontinent Sea of North America. Geology 46, 143-146.
534 doi:10.1130/G39804.1.
535 Algeo, T.J., Ingall, E., 2007. Sedimentary C_{org}: P ratios, paleocean ventilation, and
536 Phanerozoic atmospheric pO_2. Palaeogeography, Palaeoclimatology, Palaeoecology 256,
537 130–155. doi:10.1016/j.palaeo.2007.02.029.
538 Algeo, T.J., Liu, J., 2020. A re-assessment of elemental proxies for paleoredox analysis.
539 Chemical Geology 540, 119549. doi:10.1016/j.chemgeo.2020.119549.
540 Algeo, T.J., Tribovillard, N., 2009. Environmental analysis of paleoceanographic systems
541 based on molybdenum–uranium covariation. Chemical Geology 268, 211–225.
542 doi:10.1016/j.chemgeo.2009.09.001.
543 Anderson, L.A., Sarmiento, J.L., 1994. Redfield ratios of remineralization determined by
544 nutrient data analysis. Global Biogeochemical Cycles 8, 65–80. doi:10.1029/93gb03318.
545 Azrieli-Tal, I., Matthews, A., Bar-Matthews, M., Almogi-Labin, A., Vance, D., Archer, C.,
546 Teutsch, N., 2014. Evidence from molybdenum and iron isotopes and molybdenum–
547 uranium covariation for sulphidic bottom waters during Eastern Mediterranean sapropel

S1 formation. Earth and Planetary Science Letters 393, 231–242. doi:10.1016/j.epsl.2014.02.054.

Beaulieu, J.J., DelSontro, T., Downing, J.A., 2019. Eutrophication will increase methane emissions from lakes and impoundments during the 21st century. Nature Communications 10, 1375. doi:10.1038/s41467-019-09100-5.

Bond, D.P.G., Grasby, S.E., 2017. On the causes of mass extinctions. Palaeogeography, Palaeoclimatology, Palaeoecology 478, 3–29. doi:10.1016/j.palaeo.2016.11.005.

Bond, D.P.G., Sun, Y., 2020. Global Warming and Mass Extinctions Associated with Large Igneous Province Volcanism. In: Large Igneous Provinces: A Driver of Global Environmental and Biotic changes (Ernst, R.E., Dickson, A.J., Bekker, A. eds.), Wiley, pp. 89. doi:10.1002/9781119507444.ch1.

Brazier, J., Suan, G., Tacail, T., Simon, L., Martin, J.E., Mattioli, E., Balter, V., 2015. Calcium isotope evidence for dramatic increase of continental weathering during the Toarcian oceanic anoxic event (Early Jurassic). Earth and Planetary Science Letters 411, 164–176. doi:10.1016/j.epsl.2014.11.028.

Brown, J.H., Gillooly, J.F., Allen, A.P., Savage, V.M., West, G.B., 2004. Toward a metabolic theory of ecology. Ecology 85, 1771–1789. doi:10.1890/03-9000.

Bura-Nakić, E., Andersen, M.B., Archer, C., de Souza, G.F., Marguš, M., Vance, D., 2018. Coupled Mo-U abundances and isotopes in a small marine euxinic basin: Constraints on processes in euxinic basins. Geochimica et Cosmochimica Acta 222, 212-229. doi:10.1016/j.gca.2017.10.023.

Burgess, S.D., Bowring, S.A., Fleming, T.H., Elliot, D.H., 2015. High-precision geochronology links the Ferrar large igneous province with early-Jurassic ocean anoxia and biotic crisis. Earth and Planetary Science Letters 415, 90–99. doi:10.1016/j.epsl.2015.01.037.

Bush, T., Diao, M., Allen, R.J., Sinnige, R., Muyzer, G., Huisman, J., 2017. Oxic-anoxic regime shifts mediated by feedbacks between biogeochemical processes and microbial community dynamics. Nature Communication 8, 789. doi:10.1038/s41467-017-00912-x.

Calvert, S.E., Pedersen, T.F., 2007. Elemental proxies for palaeoclimatic and palaeoceanographic variability in marine sediments: interpretation and application. In: Hillaire, C., de Vernal, A. (Eds.), Proxies in Late Cenozoic Paleoceanography, vol. 1,

579 Developments in Quaternary Research. Elsevier Science, Amsterdam, pp. 567–644. doi:
580 10.1016/S1572-5480(07)01019-6.
581 Carstensen, J., Conley, D.J., Bonsdorff, E., Gustafsson, B.G., Hietanen, S., Janas, U., Jilbert,
582 T., Maximov, A., Norkko, A., Norkko, J., Reed, D.C., Slomp, C.P., Timmermann, K.,
583 Voss, M., 2014. Hypoxia in the Baltic Sea: Biogeochemical Cycles, Benthic Fauna, and
584 Management. Ambio 43, 26–36. doi:10.1007/s13280-013-0474-7.
585 Clarkson, M.O., Poulton, S.W., Guilbaud, R., Wood, R.A., 2014. Assessing the utility of Fe/Al
586 and Fe-speciation to record water column redox conditions in carbonate-rich sediments.
587 Chemical Geology 382, 111–122. doi:10.1016/j.chemgeo.2014.05.031.
588 Clarkson, M.O., Stirling, C.H., Jenkyns H.C., Dickson, A.J., Porcelli, D., Moy, C.M., Pogge
589 von Strandmann, P.A.E., Cooke, I.R., Lenton, T.M., 2018. Uranium isotope evidence for
590 two episodes of deoxygenation during Oceanic Anoxic Event 2. PNAS 115, 2918–2923.
591 doi:10.1073/pnas.1715278115.
592 Cohen, A.S., Coe, A.L., Harding, S.M., Schwark, L., 2004. Osmium isotope evidence for the
593 regulation of atmospheric CO_2 by continental weathering. Geology 32, 157–160.
594 doi:10.1130/G20158.1.
595 Dera, G., Brigaud, B., Monna, F., Laffont, R., Pucéat, E., Deconinck, J.-F., Pellenard, P.,
596 Joachimski, M.M., Durlet, C., 2011. Climatic ups and downs in a disturbed Jurassic
597 world. Geology 39, 215–218. doi:10.1130/G31579.1.
598 Duncan, R.A., Hooper, P.R., Rehacek, J., Marsh, J.S. and Duncan, A.R., 1997. The timing and
599 duration of the Karoo igneous event, southern Gondwana. Journal of Geophysical
600 Research: Solid Earth 102, 18127– 18138. doi:10.1029/97JB00972.
601 Farrimond, P., Talbot, H.M., Watson,D.F., Schulz, L.K., Wilhelms, A., 2004.
602 Methylhopanoids: molecular indicators of ancient bacteria and a petroleum correlation
603 tool. Geochimica et Cosmochimica Acta, 68, 3873– 3882. doi:10.1016/j.gca.2004.04.011.
604 Fedo, C.M., Eriksson, K.A., and Krogstad, E.J., 1996. Geochemistry of shales from the
605 Archean (similar to 3.0 Ga) Buhwa greenstone belt, Zimbabwe: Implications for
606 provenance and source-area weathering. Geochimica et Cosmochimica Acta 60, 1751–
607 1763. doi:10.1016/0016-7037(96)00058-0.
608 Feng, R.C., Wu, Y.Y., Tao, S.Z., Zhang, T.S., Yue, T., Yang, J.J., Liu, M., 2015. Sedimentary
609 microfacies characteristics and their control on reservoirs in Da'anzhai Member,Lower

610 Jurassic,Sichuan Basin. Petroleum geology and experiment 37, 320–328. doi:10.7603
611 /s40972-015-0049-8.
612 Fernandez, A., Korte, C., Ullmann, C.V., Looser, N., Wohlwend, S., Bernasconi, S.M., 2021.
613 Reconstructing the magnitude of Early Toarcian (Jurassic) warming using the reordered
614 clumped isotope compositions of belemnites. Geochimica et Cosmochimica Acta 293,
615 308–327. doi:10.1016/j.gca.2020.10.005.
616 Gilleaudeau, G.J., Algeo, T.J., Lyons, T.W., Bates, S., Anbar, A.d., 2021. Novel watermass
617 reconstruction in the Early Mississippian Appalachian Seaway based on integrated proxy
618 records of redox and salinity. Earth and Planetary Science Letters 558, 116746.
619 doi:10.1016/j.epsl.2021.116746.
620 Gómez, J.J., Comas-Rengifo, M.J., Goy, A., 2016. Palaeoclimatic oscillations in the
621 Pliensbachian (Early Jurassic) of the Asturian Basin (Northern Spain). Climate of the Past
622 Discussions 12, 1199–1214. doi:10.5194/cp-12-1199-2016.
623 Guilbaud, R., Poulton, S.W., Thompson, J., Husband, K.F., Zhu, M., Zhou, Y., Shields, G.A.,
624 Lenton, T.M., 2020. Phosphorus-limited conditions in the early Neoproterozoic ocean
625 maintained low levels of atmospheric oxygen. Nature Geoscience 13, 26–28.
626 doi:10.1038/s41561-020-0548-7.
627 Gustafsson, B.G., Schenk, F., Blenckner, T., Eilola, K., Meier, H.E., Müller-Karulis, B.,
628 Neumann, T., Ruoho,-Airola, T., Savchuk, O.P., Zorita, E., 2012. Reconstructing the
629 Development of Baltic Sea Eutrophication 1850–2006. Ambio 41, 534–548.
630 doi:10.1007/s13280-012-0318-x.
631 Günthel, M., Donis, D., Kirillin, G., Lonescu, D., Bizic, M., McGinnis, D.F., Grossart, H.,
632 Tang, K.W., 2019. Contribution of oxic methane production to surface methane emission
633 in lakes and its global importance. Nature communications 10, 5497.
634 doi:10.1038/s41467-019-13320-0.
635 Guo, Y., Yang, S., Su, N., Li, C., Yin, P., Wang, Z., 2018. Revisiting the effects of
636 hydrodynamic sorting and sedimentary recycling on chemical weathering indices.
637 Geochimica et Cosmochimica Acta 227, 48–63. doi:10.1016/j.gca.2018.02.015.
638 He, T., Corso, J.D., Newton, R.J., Wignall, P.B., Mills, B.J.W., Todaro, S., Stefano, P.D.,
639 Turner, E.C., Jamieson, R.A., Randazzo, V., Rigo, M., Jones, R.E., Dunhill, A.M., 2020.
640 An enormous sulfur isotope excursion indicates marine anoxia during the end-Triassic

mass extinction. Science Adcances 6, eabb6704. doi:10.1126/sciadv.abb6704.

He, T., Wignall, P.B., Newton, R.J., Atkinson, J.W., Keeling, J.F.J., Xiong, Y., Poulton, S.W., 2022. Extensive marine anoxia in the European epicontinental sea during the end-Triassic mass extinction. Global and Planetary Change 210, 103771. doi:10.1016/j.gloplacha.2022.1.

He, Z., Clarkson, M.O., Andersen, M.B., Archer, C., Sweere, T.C., Kraal, P., Guthauser, A., Huang, F., Vance, D., 2021. Temporally and spatially dynamic redox conditions on an upwelling margin: The impact on coupled sedimentary Mo and U isotope systematics, and implications for the Mo-U paleoredox proxy. Geochimica et Cosmochimica Acta 309, 251-271. doi:10.1016/j.gca.2021.06.024.

Hesselbo, S.P., Gröcke, D.R., Jenkyns, H.C., Bjerrum, C.J., Farrimond, P., Morgans Bell, H.S., Green, O.R., 2000. Massive dissociation of gas hydrate during a Jurassic oceanic anoxic event. Nature 406, 392–395. doi:10.1038/35019044.

Hesselbo, S.P., Jenkyns, H.C., Duarte, L.V., Oliveira, L.C.V., 2007. Carbon-isotope record of the Early Jurassic (Toarcian) Oceanic Anoxic Event from fossil wood and marine carbonate (Lusitanian Basin, Portugal). Earth and Planetary Science Letters 253, 455–470. doi:10.1016/j.epsl.2006.11.009.

Hesselbo, S.P., Pienkowski, G., 2011. Stepwise atmospheric carbon-isotope excursion during the Toarcian Oceanic Anoxic Event (Early Jurassic, Polish Basin). Earth and Planetary Science Letters 301, 365–372. doi:10.1016/j.epsl.2010.11.021.

Hinrichs, K.-U., Boetius, A., 2002. The anaerobic oxidation of methane: New insights in microbial ecology and biogeochemistry. In: Wefer, G., Billett, D., Hebbeln, D., Jørgensen, B.B., Schlüter, M., van Weering, T.C.E. (Eds.), Ocean Margin Systems. Springer-Verlag, Berlin, pp. 457– 477. doi:10.1007/978-3-662-05127-6_28.

Holba, A.G., Tegelaar, E., Ellis, L., Singletary, M.S., Albrecht, P., 2000. Tetracyclic polyprenoids: indicators of freshwater (lacustrine) algal input. Geology, 28, 251–254. doi:10.1130/0091-7613(2000)28<251:TPIOFL>2.0.CO;2.

Ivanov, A.V, Meffre, S., Thompson, J., Corfu, F., Kamenetsky, V.S., Kamenetsky, M.B., Demonterova, E.I., 2017. Timing and genesis of the Karoo-Ferrar large igneous province: New high precision U-Pb data for Tasmania confirm short duration of the major magmatic pulse. Chemical Geology 455, 32–43. doi:10.1016/j.chemgeo.2016.10.008.

672 Izumi, K., Kemp, D.B., Itamiya, S., Inui, M., 2018. Sedimentary evidence for enhanced
673 hydrological cycling in response to rapid carbon release during the early Toarcian oceanic
674 anoxic event. Earth and Planetary Science Letters 481, 162–170.
675 doi:10.1016/j.epsl.2017.10.030.
676 Jenkyns, H.C., 1985. The Early Toarcian and Cenomanian– Turonian Anoxic Events in
677 Europe: comparisons and Contrasts. Geologische Rundschau, 74, 505–518.
678 doi:10.1007/BF01821208.
679 Jenkyns, H.C., 2010. Geochemistry of oceanic anoxic events. Geochemistry Geophysics
680 Geosystems 11, Q03004. doi:10.1029/2009GC002788.
681 Jenkyns, H.C., Jones, C.E., Gröcke, D.R., Hesselbo, S.P., Parkinson, D.N., 2002.
682 Chemostratigraphy of the Jurassic System: applications, limitations and implications for
683 palaeoceanography. Journal of the Geological Society 159, 351–378. doi:10.1144/0016-
684 764901-130.
685 Jin, X., Shi, Z., Baranyi, V., Kemp, D.B., Han, Z., Luo, G., Hu, J., He, F., Chen, L., Preto, N.,
686 2020. The Jenkyns Event (early Toarcian OAE) in the Ordos Basin, North China. Global
687 and Planetary Change 194, 103273. doi:10.1016/j.gloplacha.2020.103273.
688 Jones, M.M., Ibarra, D.E., Gao,Y., Sageman. B.B., David, S., Chamberlain, C.P., Graham,
689 S.A., 2018. Evaluating Late Cretaceous OAEs and the influence of marine incursions on
690 organic carbon burial in an expansive East Asian paleo-lake. Earth and Planetary Science
691 Letters 484, 41–52. doi:10.1016/j.epsl.2017.11.046.
692 Joye, S.B., Boetius, A., Orcutt, B.N., Montoya, J.P., Schulz, H.N., Erickson, M.J., Lugo, S.K.,
693 2004. The anaerobic oxidation of methane and sulfate reduction in sediments from Gulf
694 of Mexico cold seeps. Chemical Geology 205, 219– 238.
695 doi:10.1016/j.chemgeo.2003.12.019.
696 Kemp, D.B., Coe, A.L., Cohen, A.S., Schwark, L., 2005. Astronomical pacing of methane
697 release in the Early Jurassic period. Nature 437, 396–399. doi:10.1038/nature04037
698 Kemp, D.B., Coe, A.L., Cohen, A.S., Weedon, G.P., 2011. Astronomical forcing and
699 chronology of the early Toarcian (Early Jurassic) oceanic event in Yorkshire, UK.
700 Paleoceanography 26, PA4210. doi:10.1029/2011pa002122.
701 Komar, N., Zeebe, R.E., 2017. Redox-controlled carbon and phosphorus burial: A mechanism
702 for enhanced organic carbon sequestration during the PETM. Earth and Planetary Science

703 Letters 479, 71–82. doi:10.1016/j.epsl.2017.09.011.
704 Korte, C., Hesselbo, S.P., Ullmann, C.V., Dietl, G., Ruhl, M., Schweigert, G., Thibault, N.,
705 2015. Jurassic climate mode governed by ocean gateway. Nature Communications 6,
706 10015. doi:10.1038/ncomms10015.
707 Kraal, P., Slomp, C.P., Reed, D.C., Reichart, G.J., Poulton, S.W., 2012. Sedimentary
708 phosphorus and iron cycling in and below the oxygen minimum zone of the northern
709 Arabian Sea. Biogeosciences 9, 2603–2624. doi:10.5194/bg-9-2603-2012.
710 Krencker, F.-N., Bodin, S., Suan, G., Heimhofer, U., Kabiri, L., Immenhauser, A., 2015.
711 Toarcian extreme warmth led to tropical cyclone intensification. Earth and Planetary
712 Science Letters 425, 120–130. doi:10.1016/j.epsl.2015.06.003.
713 Li, Y., He, D., 2014. Evolution of tectonic-depositional environment and prototype basins of
714 the Early Jurassic in Sichuan Basin and adjacent areas. Acta Petrolei Sinica 35, 219–232.
715 doi:10.7623/syxb201402002.
716 Li, Y.J., Feng, Y.Y., Liu, H., Zhang, L.H., Zhao, S.X., 2013, Geological characteristics and
717 resource potential of lacustrine shale gas in the Sichuan Basin, SW China. Petroleum
718 Exploration and Development 40, 454–460. doi:10.1016/S1876-3804(13)60057-9.
719 Liu, J., Cao, J., Hu, G., Wang, Y., Yang, R., Liao, Z., 2020. Water-level and redox fluctuations
720 in a Sichuan Basin lacustrine system coincident with the Toarcian OAE.
721 Palaeogeography, Palaeoclimatology, Palaeoecology 558, 109942.
722 doi:10.1016/j.palaeo.2020.109942.
723 Lu, X., Dahl, T.W., Zheng, W., Wang, S., Kendall, B., 2020. Estimating ancient seawater
724 isotope compositions and global ocean redox conditions by coupling the molybdenum
725 and uranium isotope systems of euxinic organic-rich mudrocks. Geochimica et
726 Cosmochimica Acta 290, 76-103. doi:10.1016/j.gca.2020.08.032.
727 Mattioli, E., Pittet, B., Suan, G., Mailliot, S., 2008. Calcareous nannoplankton changes across
728 the early Toarcian oceanic anoxic event in the western Tethys. Paleoceanography and
729 Paleoclimatology 23, PA3208. doi:10.1029/2007PA001435.
730 McArthur, J.M., Algeo, T.J., van de Schootbrugge, B., Li, Q., Howarth, R.J., 2008. Basinal
731 restriction, black shales, Re-Os dating, and the Early Toarcian (Jurassic) oceanic anoxic
732 event. Paleoceanography 23, PA4217. doi:10.1029/2008PA001607.
733 McElwain, J.C., Wade-Murphy, J., Hesselbo, S.P., 2005. Changes in carbon dioxide during an

734 oceanic anoxic event linked to intrusion into Gondwana coals. Nature 435, 479–482.
735 doi:10.1038/nature03618.
736 Montero-Serrano, J., Föllmi, K.B., Adatte, T., Spangenberg, J.E., Tribovillard, N., Fantasia, A.,
737 Suan, G., 2015. Continental weathering and redox conditions during the early Toarcian
738 Oceanic Anoxic Event in the northwestern Tethys: Insight from the Posidonia Shale
739 section in the Swiss Jura Mountains. Palaeogeography, Palaeoclimatology, Palaeoecology
740 429, 83–99. doi:10.1016/j.palaeo.2015.03.043.
741 Müller, T., Price, G.D., Bajnai, D., Nyerges, A., Kesjár, D., Raucsik, B., Varga, A., Judik, K.,
742 Fekete, J., May, Z., Pálfy, J., 2017. New multiproxy record of the Jenkyns Event (also
743 known as the Toarcian Oceanic Anoxic Event) from the Mecsek Mountains (Hungary):
744 Differences, duration and drivers. Sedimentology 64, 66–86. doi: 10.1111/sed.12332.
745 Nesbitt, H.W., Young, G.M., 1982. Early Proterozoic climates and plate motions inferred from
746 major element chemistry of lutites. Nature 299, 715–717. doi: 10.1038/299715a0.
747 O'Beirne, M.D., Werne, J.P., Hecky, R.E., Johnson, T.C., Katsev, S., Reavie, E.D., 2017.
748 Anthropogenic climate change has altered primary production in Lake Superior. Nature
749 Communications 8, 15713. doi:10.1038/ncomms15713.
750 Pálfy, J., Smith, P.L., 2000. Synchrony between Early Jurassic extinction, oceanic anoxic
751 event, and the Karoo-Ferrar flood basalt volcanism. Geology 28,747–750. doi:
752 10.1130/0091-7613(2000)282.0.CO;2.
753 Panahi, A. and Young, G.M., 1997. A geochemical investigation into the provenance of the
754 Neoproterozoic Port Askaig Tillite, Dalradian Supergroup, western Scotland.
755 Precambrian Research 85, 81–96. doi:10.1016/S0301-9268(97)00033-8.
756 Percival, L.M.E., Cohen, A.S., Davies, M.K., Dickson, A.J., Hesselbo, S.P., Jenkyns, H.C.,
757 Leng, M.J., Mather, T.A., Storm, M.S., Xu, W., 2016. Osmium isotope evidence for two
758 pulses of increased continental weathering linked to Early Jurassic volcanism and climate
759 change. Geology 44, 759–762. doi:10.1130/G37997.1.
760 Percival, L.M.E., Witt, M.L.I., Mather, T.A., Hermoso, M., Jenkyns, H.C., Hesselbo, S.P., Al-
761 Suwaidi, A.H., Storm, M.S., Xu,W., Ruhl, M., 2015. Globally enhanced mercury
762 deposition during the end-Pliensbachian extinction and Toarcian OAE: A link to the
763 Karoo–Ferrar Large Igneous Province. Earth and Planetary Science Letters 428, 267–
764 280. doi:10.1016/j.epsl.2015.06.064.

765 Pittet, B., Suan, G., Lenoir, F., Duarte, L.V., Mattioli, E., 2014. Carbon isotope evidence for
766 sedimentary discontinuities in the lower Toarcian of the Lusitanian Basin (Portugal): sea
767 level change at the onset of the Oceanic Anoxic Event. Sedimentary Geology 303, 1–14.
768 doi:10.1016/j.sedgeo.2014.01.001.
769 Poulton, S.W., Canfield, D.E., 2005. Development of a sequential extraction procedure for
770 iron: Implications for iron partitioning in continentally derived particulates. Chemical
771 Geology 214, 209–221. doi:10.1016/j.chemgeo.2004.09.003.
772 Poulton, S.W., Canfield, D.E., 2011. Ferruginous Conditions: A Dominant Feature of the
773 Ocean through Earth's History. Elements 7, 107–112. doi:10.2113/gselements.7.2.107.
774 Poulton, S.W., Raiswell, R., 2002. The low temperature geochemical cycle of iron: From
775 continental fluxes to marine sediment deposition. American Journal of Science 302, 774-
776 805. doi:10.2475/ajs.302.9.774.
777 Poulton, S. W. 2021. The Iron Speciation Paleoredox Proxy. The Iron Speciation Paleoredox
778 Proxy 6454, (Cambridge University Press). doi:10.1017/9781108847148.
779 Raiswell, R., Canfield, D.E., 2012. The Iron Biogeochemical Cycle Past and Present.
780 Geochemical Perspect. 1, 1–220. doi:10.7185/geochempersp.1.1.
781 Reed, D.C., Gustafsson, B.G., Slomp, C.P., 2016. Shelf-to-basin iron shuttling enhances
782 vivianite formation in deep Baltic Sea sediments. Earth and Planetary Science Letters
783 434, 241–251. doi:10.1016/j.epsl.2015.11.033.
784 Reinhard, C.T., Planavsky, N., 2020. Biogeochemical Controls on the Redox Evolution of
785 Earth's Oceans and Atmosphere. Elements 16, 191–196.
786 doi:10.2138/gselements.16.3.191.
787 Reolid, M., Copestake, P., Johnson, B., 2019. Foraminiferal assemblages, extinctions and
788 appearances associated with the Early Toarcian Oceanic Anoxic Event in the Llanbedr
789 (Mochras Farm) Borehole, Cardigan Bay Basin, United Kingdom. Palaeogeography,
790 Palaeoclimatology, Palaeoecology 532, 109277. doi:10.1016/j.palaeo.2019.109277.
791 Reolid, M., Mattioli, E., Duarte, L.V., Marok, A., 2020. The Toarcian Oceanic Anoxic Event
792 and the Jenkyns Event (IGCP-655 final report). Episodes 43.
793 doi:10.18814/epiiugs/2020/020051.
794 Reolid, M., Mattioli, E., Duarte, L.V., Ruebsam, W., 2021. The Toarcian Oceanic Anoxic
795 Event: where do we stand? Geological Society London Special Publications 514, 1–11.

doi:10.1144/SP514-2021-74.

Rita, P., Reolid, M., Duarte, L.V., 2016. Benthic foraminiferal assemblages record major environmental perturbations during the Late Pliensbachian–Early Toarcian interval in the Peniche GSSP, Portugal. Palaeogeography, Palaeoclimatology, Palaeoecology 454, 267–281. doi:10.1016/j.palaeo.2016.04.039.

Robinson, S.A., Heimhofer, U., Hesselbo, S.P., Petrizzo, M.R., 2017. Mesozoic climates and oceans – a tribute to Hugh Jenkyns and Helmut Weissert. Sedimentology 64, 1–15. doi:10.1111/sed.12349.

Rothman, D.H., 2017. Thresholds of catastrophe in the Earth system. Science Advances. 3, e1700906. doi:10.1126/sciadv.1700906.

Rudnick, R.L., Gao, S., 2014. Composition of the continental crust. In: Treatise on Geochemistry. Elsevier, pp. 1–51. doi:10.1016/B978-0-08-095975-7.00301-6.

Ruebsam, W., Reolid, M., Sabatino, N., Masetti, D., Schwark, L., 2020. Molecular paleothermometry of the early Toarcian climate perturbation. Global and Planetary Change 195, 103351. doi:10.1016/j.gloplacha.2020.103351.

Schobben, M., Foster, W.J., Sleverland, A.R.N., Zuchuat, V., Svensen, H.H., Planke, S., Bond, D.P.G., Marcelis, F., Newton, R.J., Wignall, P.B., Poulton, S.W., 2020. A nutrient control on marine anoxia during the end-Permian mass extinction. Nature Geoscience 13, 640–646. doi:10.1038/s41561-020-0622-1.

Scholz, F., 2018. Identifying oxygen minimum zone-type biogeochemical cycling in Earth history using inorganic geochemical proxies. Earth-Science Reviews 184, 29–45. doi:10.1016/j.earscirev.2018.08.002.

Scotese, C.R., Song, H., Mills, J.W., van der Meer, D.G., 2021. Phanerozoic paleotemperatures: The earth's changing climate during the last 540 million years. Earth-Science Reviews 215, 103503. doi:10.1016/j.earscirev.2021.103503.

Seidel, L., Broman, E., Turner, S., Ståhle, M., Dopson, M., 2021. Interplay between eutrophication and climate warming on bacterial communities in coastal sediments differs depending on water depth and oxygen history. Scientific Reports 11, 23384. doi:10.1038/s41598-021-02725-x.

Stüeken, E.E., Martinez, A., Love, G., Olsen, P.E., Bates, S., Lyons, T.W., 2019. Effects of pH on redox proxies in a Jurassic rift lake: Implications for interpreting environmental

827 records in deep time. Geochimica et Cosmochimica Acta 252, 240-267.
828 doi:10.1016/j.gca.2019.03.014.
829 Suan, G., Mattioli, E., Pittet, B., Lécuyer, C., Suchéras-Marx, B., Duarte, L.V., Phillipe, M.,
830 Reggiani, L., Martineau, F., 2010. Secular environmental precursors to early Toarcian
831 (Jurassic) extreme climate changes. Earth and Planetary Science Letters 290, 448–458.
832 doi:10.1016/j.epsl.2009.12.047.
833 Suan, G., van de Schootbrugge, B., Adatte, T., Fiebig, J., Oschmann, W., 2015. Calibrating the
834 magnitude of the Toarcian carbon cycle perturbation. Paleoceanography 30,495–509.
835 doi:10.1002/2014PA002758.
836 Svensen, H., Planke, S., Chevallier, L., Malthe-Sorenssen, A., Corfu, F. and Jamtveit, B.,
837 2007. Hydrothermal venting of greenhouse gases triggering Early Jurassic global
838 warming. Earth and Planetary Science Letters 256, 554–566.
839 doi:10.1016/j.epsl.2007.02.013.
840 Them, T.R., Gill, B.C., Caruthers, A.H., Gerhardt, A.M., Gröcke, D.R., Lyons, T.W.,
841 Marroquin, S.M., Nielsen, S.G., Alexandre, J.P.T., Owens, J.D., 2018. Thallium isotopes
842 reveal protracted anoxia during the Toarcian (Early Jurassic) associated with volcanism,
843 carbon burial, and mass extinction. PNAS 115, 6596–6601.
844 doi:10.1073/pnas.1803478115.
845 Them, T.R., Gill, B.C., Selby, D., Gröcke, D.R., Friedman, R.M., Owens, J.D., 2017. Evidence
846 for rapid weathering response to climatic warming during the Toarcian Oceanic Anoxic
847 Event. Scientific Reports 7, 5003. doi:10.1038/s41598-017-05307-y.
848 Tribovillard, N., Algeo, T.J., Lyons, T., Riboulleau, A., 2006. Trace metals as paleoredox and
849 paleoproductivity proxies: An update. Chemical Geology 232, 12–32.
850 doi:10.1016/j.chemgeo.2006.02.012.
851 Tribovillard, N., Bout-Roumazeilles, V., Algeo, T., Lyons, T.W., Sionneau, T., Montero-
852 Serrano, J.C., Riboulleau, A., Baudin, F., 2008. Paleodepositional conditions in the Orca
853 Basin as inferred from organic matter and trace metal contents. Marine Geology 254, 62–
854 72. doi:10.1016/j.margeo.2008.04.016.
855 Tribovillard, N., du Châtelet, E.A., Gay, A., Barbecot, F., Sansjofre, P., Potdevin, J.-L., 2013.
856 Geochemistry of cold seepage-impacted sediments: Per-ascensum or per-descensum trace
857 metal enrichment? Chemical Geology 340, 1–12. doi:10.1016/j.chemgeo.2012.12.012.

Wang, Z., Zou, C., Tao, S., Li, J., Wang, S., Zhao, C., 2004. Analysis on tectonic evolution and exploration potential in Dabashan foreland basin. Acta Petrolei Sinica 25, 23–28. doi:10.7623/syxb200406005.

Welander, P.V., Summons, R.E., 2012. Discovery, taxonomic distribution, and phenotypic characterization of a gene required for 3-methylhopanoid production. Proceedings of the National Academy of Sciences of the United States of America, 109, 12905–12910. doi:10.1073/pnas.1208255109.

Woolway, R.L., Sharma, S., Weyhenmeyer, G.A., Debolskiy, A., Golub, M. et al., 2021. Phenological shifts in lake stratification under climate change. Nature Communications 12, 2318. doi:10.1038/s41467-021-22657-4.

Xiong, Y., Guilbaud, R., Peacock, C.L., Cox, R.P., Canfield, D.E., Krom, M.D., Poulton, S.W., 2019. Phosphorus cycling in Lake Cadagno, Switzerland: A low sulfate euxinic ocean analogue. Geochimica et Cosmochimica Acta 251, 116–135. doi:10.1016/j.gca.2019.02.011.

Xu, Q., Liu, B., Ma, Y., Song, X., Wang, Y., Xin, X., 2017a. Controlling factors and dynamical formation models of lacustrine organic matter accumulation for the Jurassic Da'anzhai Member in the central Sichuan Basin, southwestern China. Marine and Petroleum Geology 86, 1391–1405. doi:10.1016/j.marpetgeo.2017.07.014.

Xu, W., Ruhl, M., Jenkyns, H.C., Hesselbo, S.P., Riding, J.B., Selby, D., Naafs, B.D.A., Weijers, J.W.H., Pancost, R.D., Tegelaar, E.W., Idia, E.F., 2017b. Carbon sequestration in an expanded lake system during the Toarcian oceanic anoxic event. Nature Geoscience 10, 129–134. doi:10.1038/ngeo2871.

Xu, W., Ruhl, M., Jenkyns, H.C., Leng, M.J., Huggett, J.M., Minisini, D., Ullmann, C.V., Riding, J.B., Weijers, J.W.H., Storm, M.S., Percival, L.M.E., Tosca, N.J., Idiz, E.F., Tegelaar, E.W., Hesselbo, S.P., 2018. Evolution of the Toarcian (Early Jurassic) carbon-cycle and global climatic controls on local sedimentary processes (Cardigan Bay Basin, UK). Earth and Planetary Science Letters 484, 396–411. doi:10.1016/j.epsl.2017.12.037.

Xu, W., Weijers, J.W.H., Ruhl, M., Idiz, E.F., Jenkyns, H.C., Riding, J.B., Gorbanenko, O., Hesselbo, S.P., 2021. Molecular and petrographical evidence for lacustrine environmental and biotic change in the palaeo-Sichuan mega-lake (China) during the Toarcian Oceanic Anoxic Event. Geological Society of London Publications.

889 doi:10.6084/m9.figshare.c.5433544.
890 Yankova, Y., Neuenschwander, S., Köster, O., Posch, T., 2017. Abrupt stop of deep water
891 turnover with lake warming: drastic consequences for algal primary producers. Scientific
892 Reports 3, 13770. doi:10.1038/s41598-017-13159-9.
893 Young, G.M. and Nesbitt, H.W., 1999. Paleoclimatology and provenance of the glaciogenic
894 Gowganda Formation (Paleoproterozoic), Ontario, Canada: A chemostratigraphic
895 approach. Geological Society of America Bulletin 111, 264–274. doi:10.1130/0016-
896 7606(1999)1112.3.CO;2.
897 Zakem, E.J., Polz, M.F., Follows, M.J., 2020. Redox-informed models of global
898 biogeochemical cycles. Nature Communications 11, 5680. doi:10.1038/s41467-020-
899 19454-w.
900 Zheng, R., 1998. High-Resolution Sequence Stratigraphy of Da'anzhai Formation, Lower
901 Jurassic in Sichuan Basin. Act Sedimentologic Sinica 16, 42–49.
902 doi:CNKI:SUN:CJXB.0.1998-02-008.
903 Zhao, W. Z., Wang, H. J., Xu, C. C., Bian, C. S., Wang, Z. C., Gao, X. H., 2010. Reservoir-
904 forming mechanism and enrichment conditions of the extensive Xujiahe Formation gas
905 reservoirs, central Sichuan Basin. Petroleum Exploration and Development 37, 146-157.
906 doi:10.1016/S1876-3804(10)60022-5.
907 Zhu, Y. M., Hao, F., Zou, H. Y., Cai, X.Y., Luo, Y., 2007. Jurassic oils in the central Sichuan
908 basin, southwest China: Unusual biomarker distribution and possible origin. Organic
909 Geochemistry 38, 1884-1896. doi:10.1016/j.orggeochem.2007.06.016.
910
911

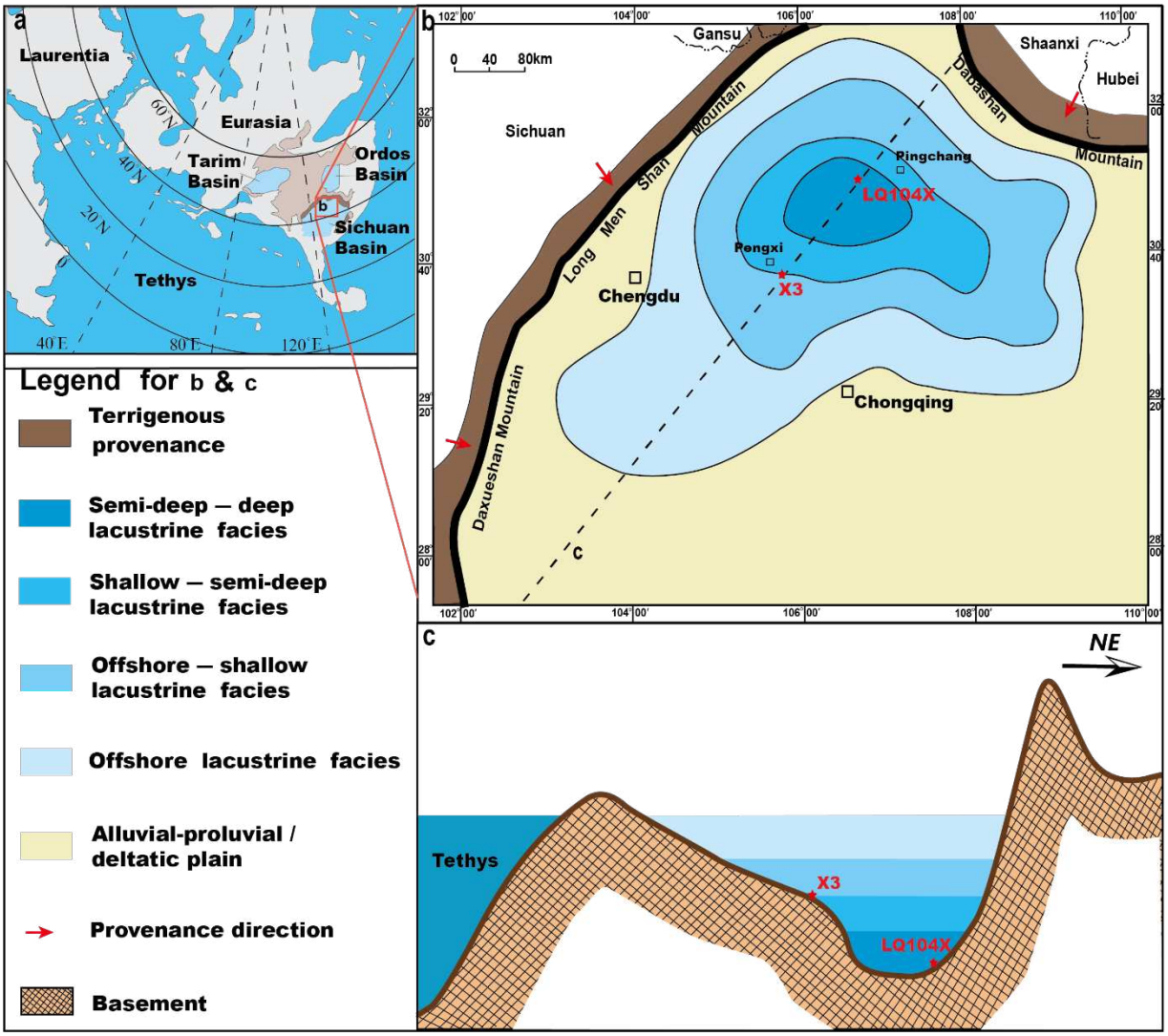

Fig. 1. Geological map of the Sichuan Basin during the Early Jurassic. a. Location of the Sichuan Basin in the Eurasia continent (modified after Xu et al., 2017a). **b.** Sedimentary environment of the Toarcian Sichuan Basin and the paleogeographic locations of X3 and LQ104X wells. **c.** Bathymetric positions of X3 and LQ104X wells in the lacustrine Sichuan Basin.

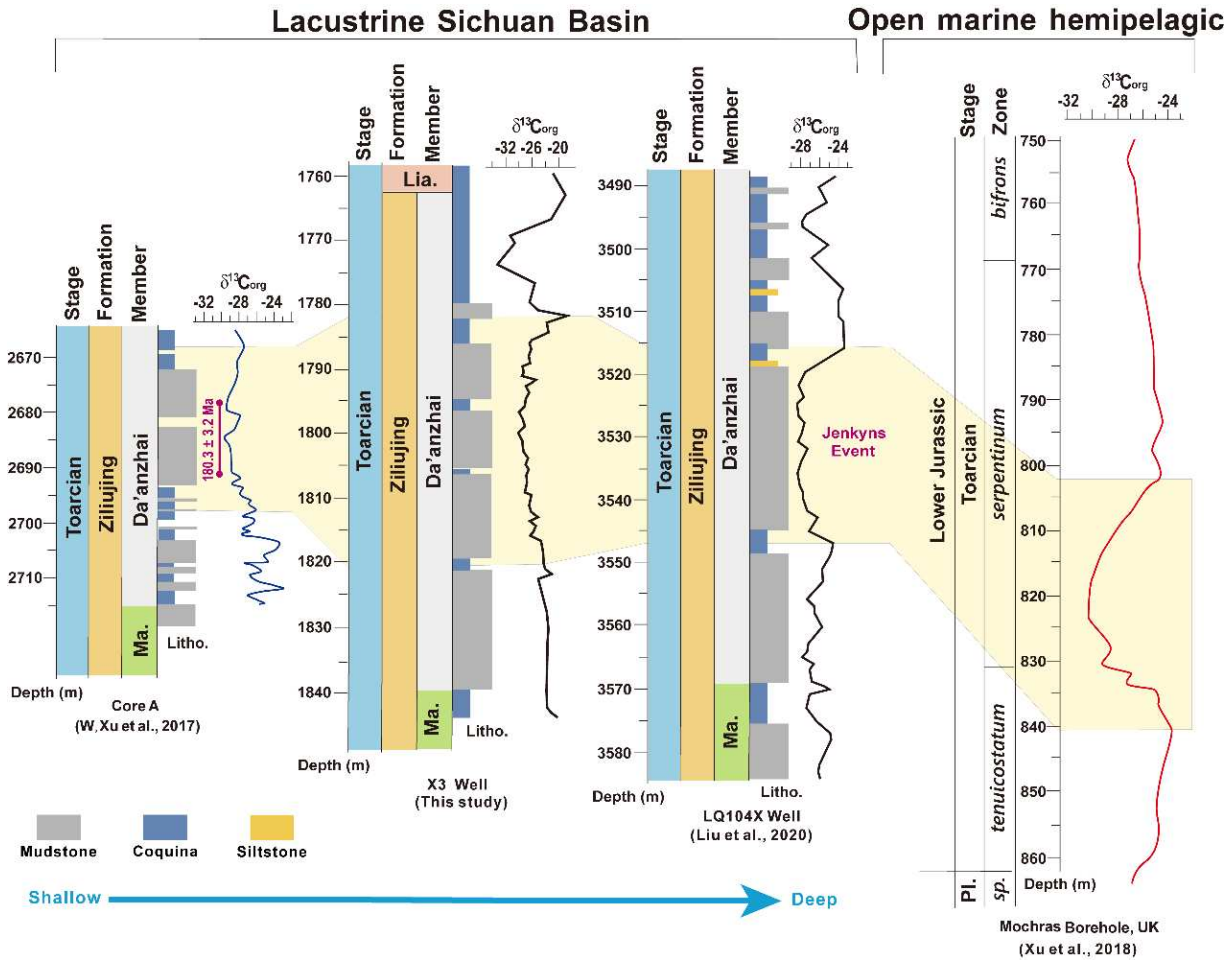

Fig. 2. Interbasinal and global stratigraphic correlation of Toarcian strata using organic carbon isotope data of bulk sediment. Data of X3 well are reported in this study. Data of LQ104X well are presented from Liu et al. (2020) of the lacustrine Sichuan Basin. Data of Core A in the Sichuan Basin are presented from Xu et al. (2017). Data of the open-marine hemipelagic Mochras core shows a reference of $\delta^{13}C_{org}$ profile of western Tethys (Xu et al., 2018). The yellow shaded area represents the duration of the Jenkyns Event. The age of the Da'anzhai Member (180.3 ± 3.2 Ma) was given by Re–Os dating (Xu et al., 2017). Note: Ma. – Ma'anshan Member; Lia. – Lianggaoshan Formation; Pl. – Pliensbachian Stage; *sp.* – *spinatum zone.*

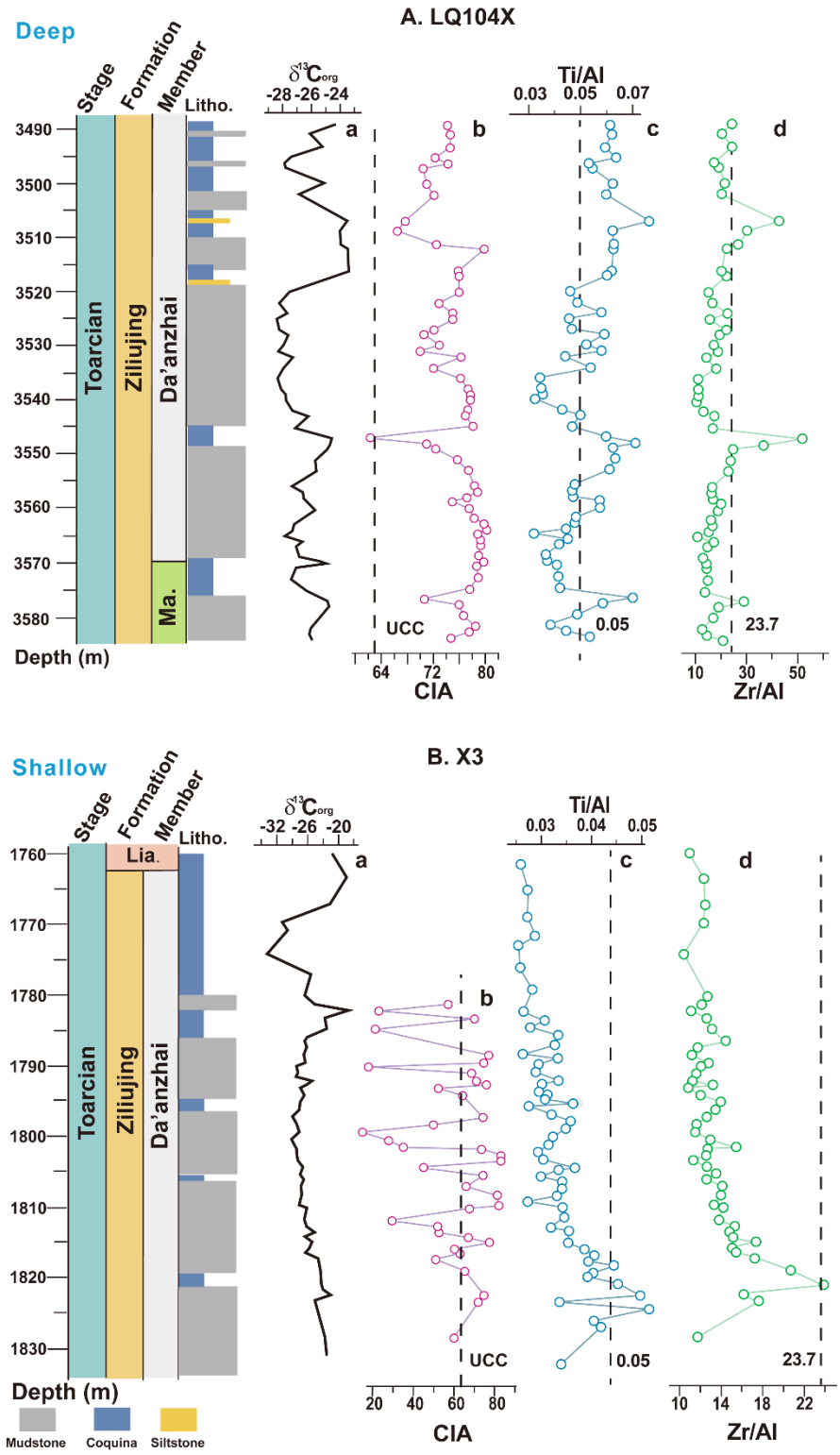

Fig. 3. Variation of chemical index of alteration in the Toarcian Ziliujing Formation of the lacustrine Sichuan Basin. A. deep water LQ104X well. **B.** shallower X3 well. **a.** Organic carbon isotope profiles of bulk sediment. **b.** Chemical index of alteration (CIA). **c.** Ti/Al ratio. **d.** Zr/Al ratio. The vertical dotted lines represent the CIA, Ti/Al and Zr/Al values of the UCC (upper continental crust; Rudnick and Gao, 2014).

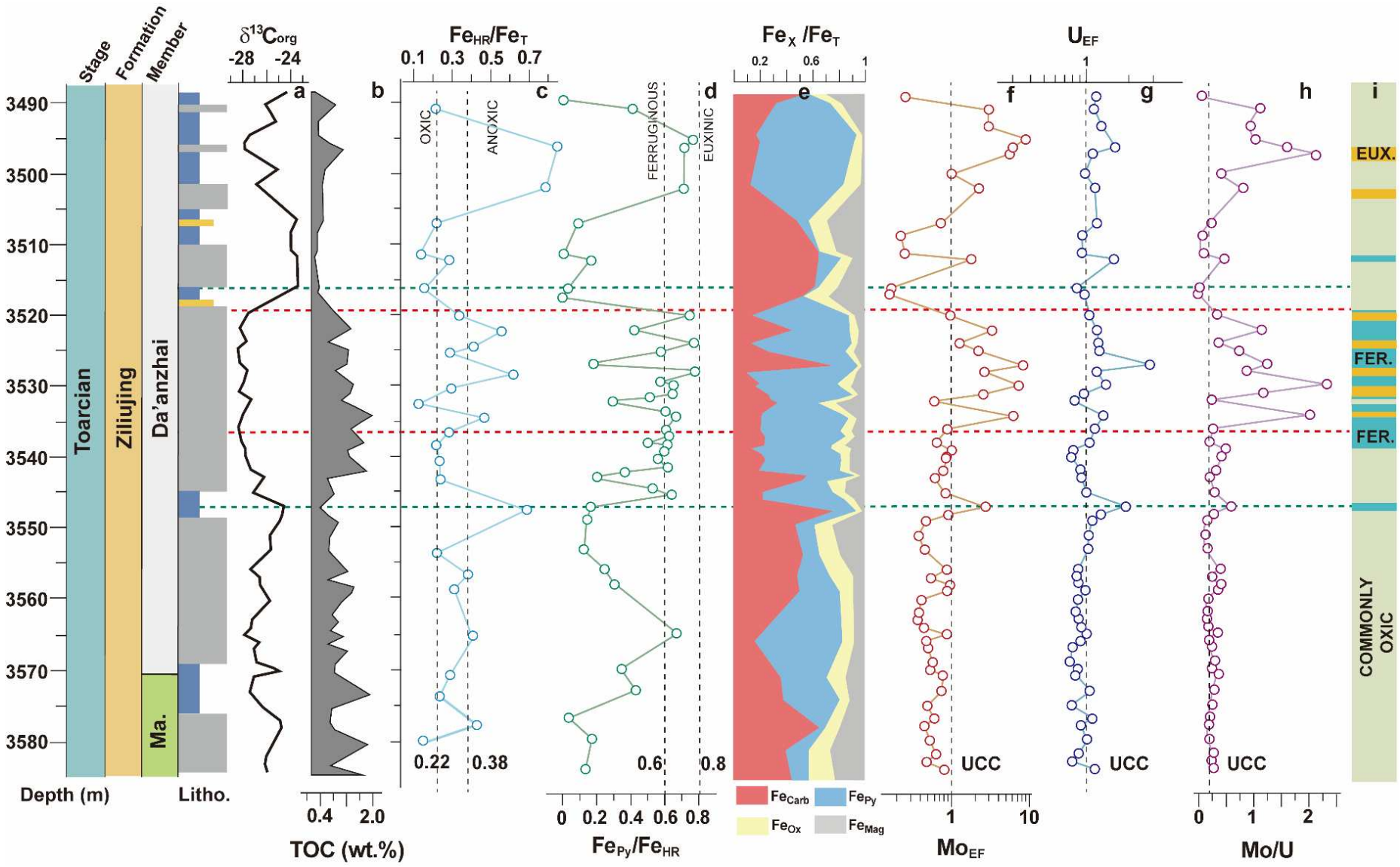

Fig. 4. Variation of carbon, iron and trace metal geochemistry from the deep water LQ104X well. Green horizontal dotted lines represent the initiation and termination of the Jenkyns Event. Red horizontal dotted lines represent the start and end of sedimentary Mo enrichment. We

aware that these marine-based Fe speciation thresholds may vary in different lacustrine settings, but they are shown here for comparison. **a.** Organic carbon isotope profiles of bulk sediment. **b.** Total organic carbon (TOC) contents. **c.** Highly reactive iron to total iron ratios (Fe_{HR}/Fe_T); vertical dash lines represent the thresholds for oxic ($Fe_{HR}/Fe_T < 0.22$) and anoxic ($Fe_{HR}/Fe_T > 0.38$), respectively; area between 0.22 – 0.38 represents either oxic or anoxic conditions. **d.** Pyrite iron to highly reactive iron ratios (Fe_{Py}/Fe_{HR}); vertical dash lines represent the thresholds for ferruginous ($Fe_{Py}/Fe_{HR} < 0.6$) and euxinic ($Fe_{Py}/Fe_{HR} > 0.8$), respectively; area between 0.6 – 0.8 represents either ferruginous oreuxinic conditions. **e.** Proportion of individual reactive iron specie within the total highly reactive iron pool. **f.** Enrichment of molybdenum. **g.** Enrichment of uranium. Vertical dashed lines in figures **f and g** represent the enrichment of Mo and U in UCC, respectively. **h.** Mo to U ratios; vertical dashed lines represent the Mo to U ratios in UCC. **i.** Variation in water column redox conditions; lime-green band – commonly oxic condition; lake blue band – commonly anoxic-ferruginous condition; orange band – commonly euxinic condition.

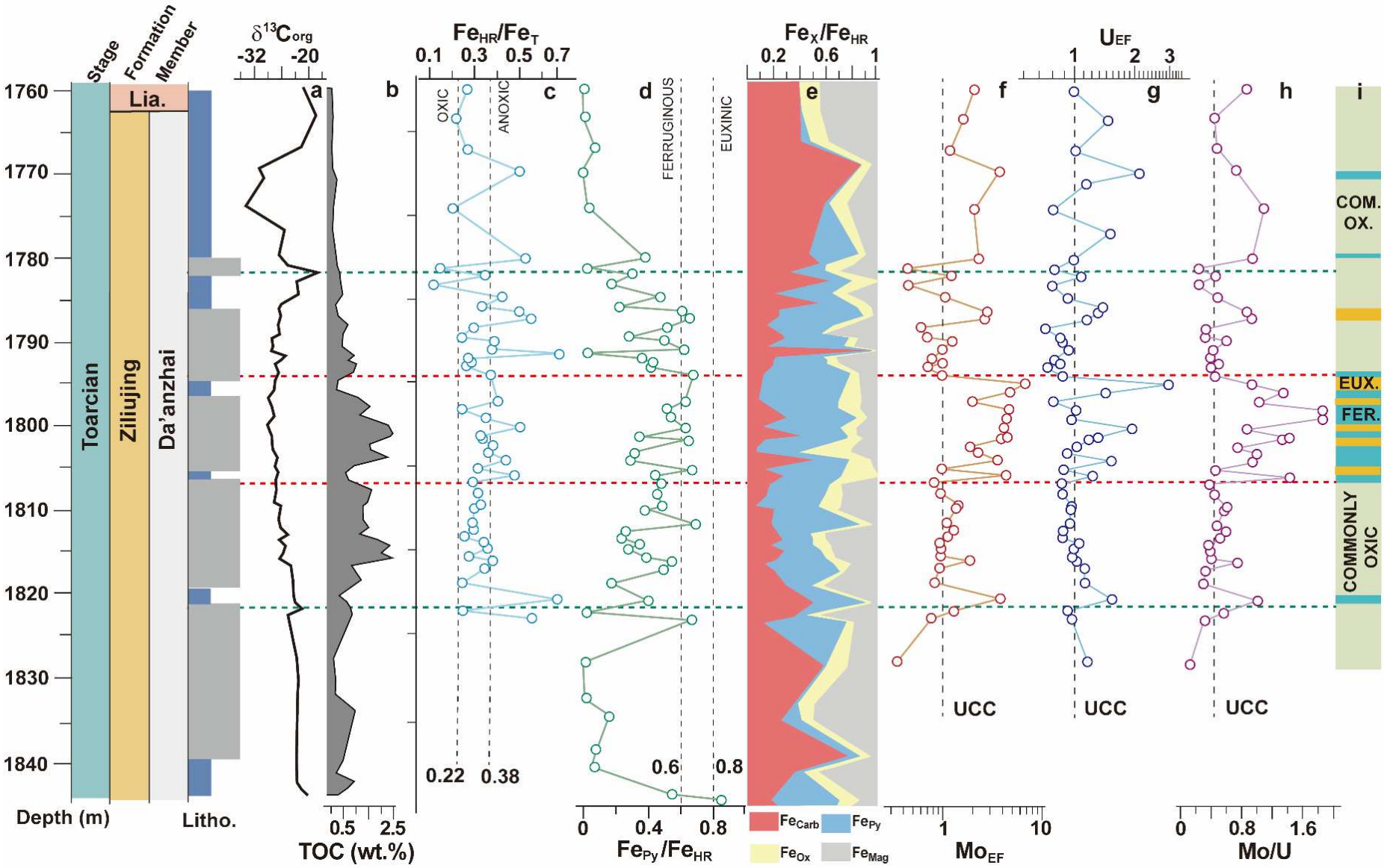

Fig. 5. Variation of carbon, iron and trace metal geochemistry from the shallower X3 well. Green horizontal dotted lines represent the initiation and termination of the Jenkyns Event. Red horizontal dotted lines represent the strat and end of sedimentary Mo enrichment. **a.** Organic

carbon isotope profiles of bulk sediment. **b.** TOC contents. **c.** Fe_{HR}/Fe_T. **d.** Fe_{Py}/Fe_{HR}. **e.** The proportion of each reactive iron speciation within the total highly reactive iron pool. **f.** Enrichment of molybdenum. **g.** Enrichment of uranium. **h.** Mo to U ratio. **i.** Variation in water-column redox conditions.

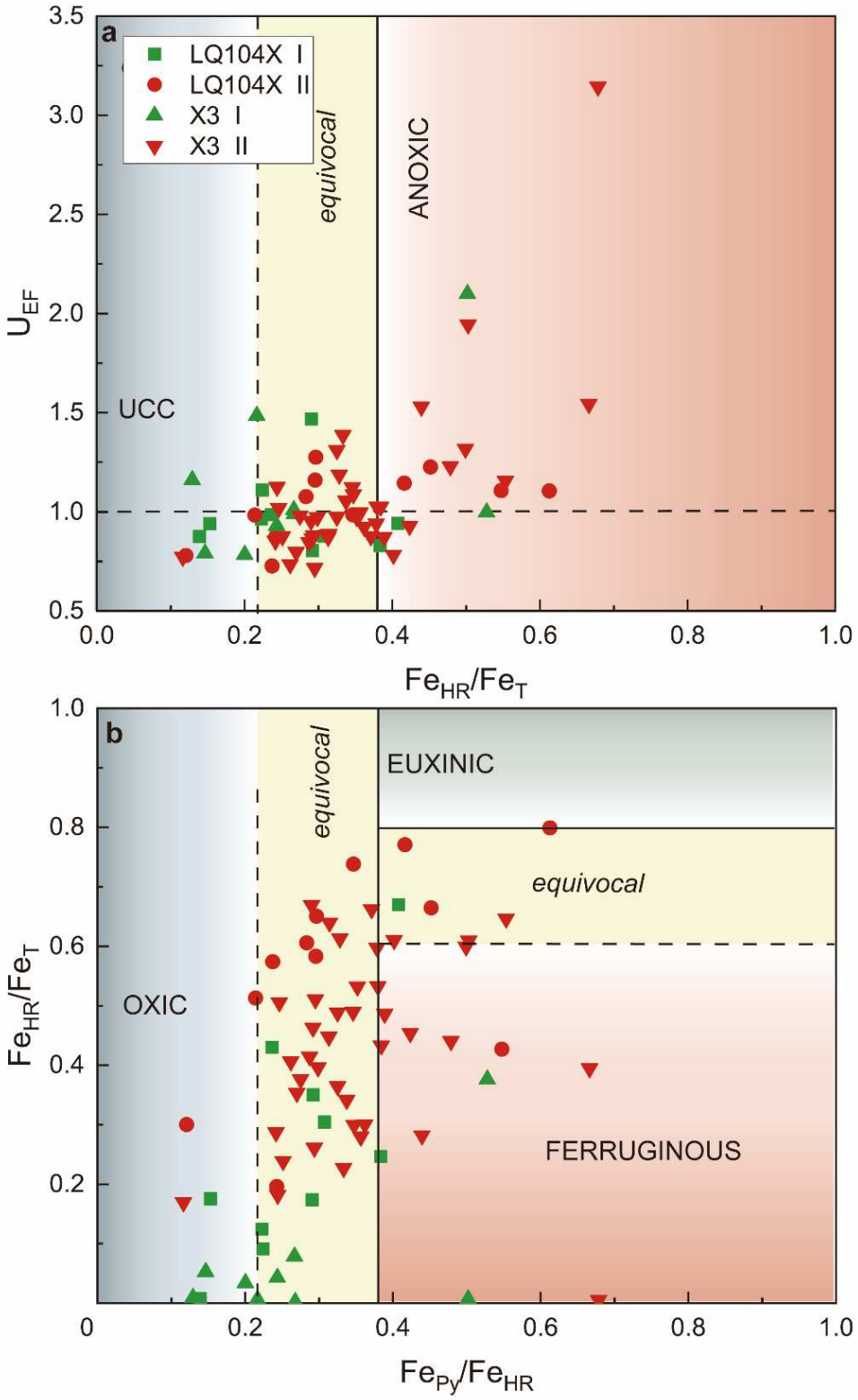

Fig. 6. Fe speciation and U enrichment in the Toarcian Da'anzhai Member from the Sichuan Basin. a. Cross-plot of U_{EF} versus Fe_{HR}/Fe_T ratio. The horizontal dash line represents the U enrichment of UCC (Rudnick and Gao, 2014). **b.** Cross-plot of Fe_{Py}/Fe_{HR} ratio against Fe_{HR}/Fe_T ratio. Fe_{HR}/Fe_T ratios of > 0.38 represent anoxic condition, whereas < 0.22 represent oxic water column (Poulton and Raiswell, 2002; Poulton, 2021). Fe_{Py}/Fe_{HR} values > 0.8 are

indicative of water column euxinia, whereas < 0.6 represent ferruginous condition (Poulton, 2021). Additionally, the yellow shade area (i.e., 0.22 < Fe_{HR}/Fe_T < 0.38 and 0.6 < Fe_{Py}/Fe_{HR} < 0.8) may be equivocal, which can represent either oxic or anoxic conditions, and ferruginous or euxinic conditions, respectively (Poulton, 2021). The LQ104X I and X3 I represent the samples in non-Jenkyns Event intervals, while the LQ104X II and X3 II represent the samples in Jenkyns Event intervals. Note that samples deposited under anoxic conditions show obvious covariation between their U_{EF} and Fe_{HR}/Fe_T ratios (r^2 = 0.40).

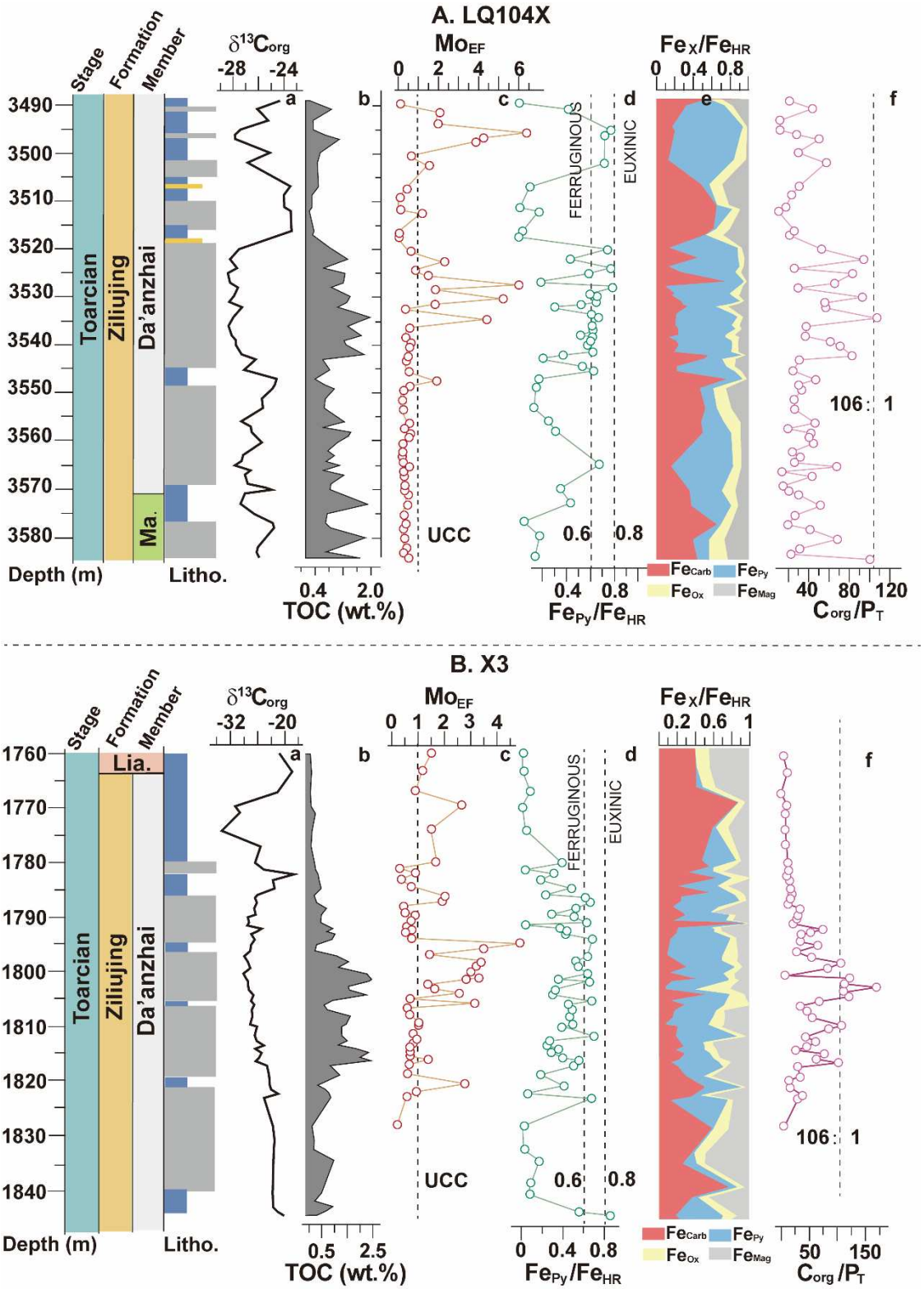

Fig. 7. Variation of redox proxies and P cycling in the Toarcian Da'anzhai Member from the Sichuan Basin. A. deep water LQ104X well. **B.** shallower X3 well. **a**. Organic carbon isotope profiles of bulk sediment. **b.** Total organic carbon (TOC) contents. **c.** Enrichment of molybdenum. **d.** Pyrite iron to highly reactive iron ratios (Fe_{Py}/Fe_{HR}). **e.** Proportion of each reactive iron speciation within the total highly reactive iron pool. **f**. Molar ratio of organic carbon to total phosphorus (Refield ratio; Algeo and Ingall, 2007).

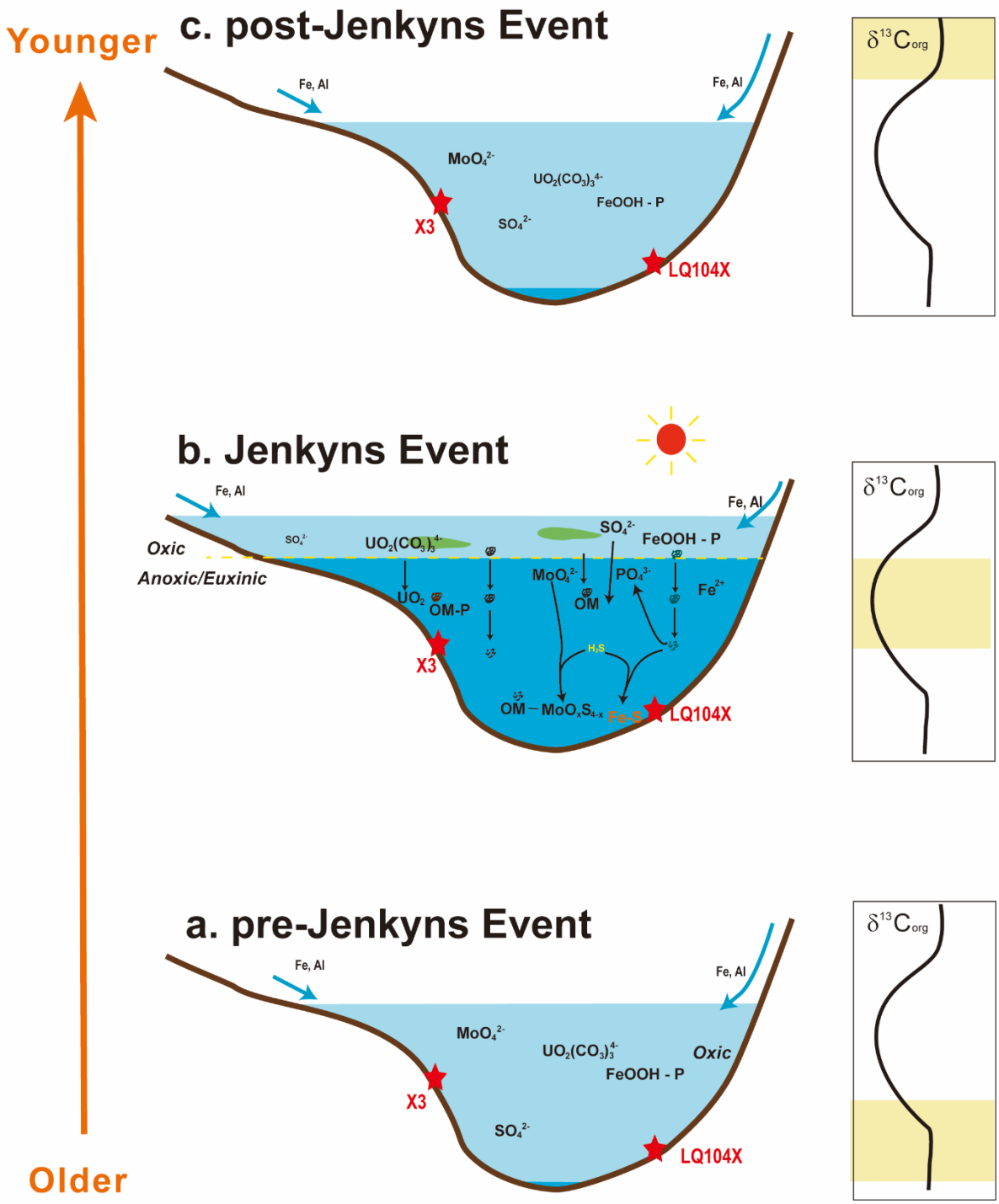

Fig. 8. Conceptual model of lacustrine redox changes in the Sichuan Basin across the Jenkyns Event. Yellow bands through data profiles indicate different episodes of the early Toarcian negative carbon isotope excursion event. **a.** dominantly oxic condition in the basin during pre-Jenkyns Event interval. **b.** heyday of the Jenkyns Event, when the LQ104X site and X3 site are situated below the chemocline with dominantly anoxic-ferruginous or euxinic conditions. **c** post-Jenkyns Event interval dominated by oxic condition at both sites, but interspersed with short-lived anoxic pulses. The "sun" represents hyperthermal event.